The Timing of Global Floods and its Association with Climate and Topography

P. Torre Zaffaroni[1,2,3], G. Baldi[3], M. Texeira[1,2], C.M. Di Bella[1,2], and E.G. Jobbágy[3]

[1]Instituto de Investigaciones Fisiológicas y Ecológicas Vinculadas a la Agricultura (IFEVA), Facultad de Agronomía, Universidad de Buenos Aires, CONICET, Buenos Aires, Argentina
[2]Departamento de Métodos Cuantitativos y Sistemas de Información, Facultad de Agronomía, Universidad de Buenos Aires
[3]Grupo de Estudios Ambientales – IMASL, Universidad Nacional de San Luis & CONICET, San Luis, Argentina

Key Points:

- Topography is more important than climate in explaining the global distribution of floods;
- Floods are more seasonal in equatorial and boreal climates and more unpredictable in arid lowlands and the subtropical and temperate belt;
- Over the last 30 years, near a tenth of the Earth's land experienced long-term flooding increases, while <2% saw net decreases

Corresponding author: Paula Torre Zaffaroni, `torrezaffaroni@agro.uba.ar`

Abstract

Until recently, the development of a global geography of floods was challenged by the fragmentation and heterogeneity of in situ data and the high costs of processing large amounts of remote sensing data. Such geography would facilitate the exploration of large-scale drivers of flood extent and timing including wide latitudinal, climate, and topographic effects. Here we used a monthly dataset spanning 30 years (Global Surface Water Extent) to develop a worldwide geographical characterization of slow floods (1-degree grid), weighting the relative contribution of seasonal, interannual, and long-term fluctuations on overall variability, and quantifying precipitation-flooding delays where seasonality dominated. We explored the dominance of different flooding timings across five Köppen-Geiger main climates and seven topography classes derived from modeled water table depths (i.e., hydro-topography) to contribute top-down insight about the outstanding, cross-regional flooding patterns and their likely large-scale drivers. Our results showed that, globally, the mean extent of floods averaged 0.48% of the global land area, predominantly associated with hydro-topography (>2x more extensive in flatter landscapes). Climate drove flood timings, with predictable, seasonally-dominated fluctuations in cold regions, interannual and mixed patterns in temperate climates, and more irregular (higher variability) and unpredictable (less seasonal) patterns in arid regions. Net gains of flooded area dominated temporal variability in 9% of the cells including boreal clusters likely affected by warming trends. We propose that this new geographical perspective of floods can aid different avenues of hydrological research in the upscaling and extrapolation of field studies and the parsimonious representation of floods in hydroclimatic models.

1 Introduction

Floods influence a myriad of biophysical and human processes at multiple spatial and temporal scales, examples of which are nutrient cycles in riverine environments, primary productivity and ecological succession in wetlands, and local climate properties (Aufdenkampe et al., 2011; Davies et al., 2008; Faysse et al., 2020; Houspanossian et al., 2018; Jardine et al., 2015; Robertson et al., 2001; Sanchis et al., 2012; Simões et al., 2013; Loarie et al., 2011). The temporal dynamics of floods modulate these influences and may be described according to regimes and timings. Flood regimes have been defined through their association with different triggers, i.e., rainfall pulses, snowmelt, runoff from upslope areas, and soil moisture (R. Merz & Blöschl, 2003; Parajka et al., 2010), and through the level of sensitivity to terrain or atmospheric properties, i.e., hydraulic infrastructure, land use and land cover changes, and climatic changes (Sivapalan, 2005; Prigent et al., 2007; Silva et al., 2017; B. Merz et al., 2021). Flood timing, instead, describes the moment, duration, and degree of periodicity of flooding peaks (e.g. summer vs. winter-time floods, flash floods lasting days vs. slow floods lasting months, seasonal vs. erratic floods). It is also characterized according to their recurrence and degree of extremeness (e.g., 1- vs. 100-year), and rich/poor flooding periods lasting several years (Cunderlik et al., 2004; Hall et al., 2014; Lee et al., 2015; R. Merz & Blöschl, 2003; Pickens et al., 2020; Saharia et al., 2017; Tulbure & Broich, 2019; Warfe et al., 2011). Thus, and from a systems theory framework (O'Neill et al., 1986), we could distinguish scale-dependent factors influencing these two aspects of flooding dynamics. From a bottom-up perspective, we can view flooding regimes as the result of different processes (i.e., causal mechanisms). In turn, from a top-down perspective, we can think of the dominating timescale at which flooding fluctuates (hereby, flood timing; for example, seasons, years and even decades) as indicators of the influence of drivers that (i) operate at larger spatial scales (e.g., climate regimes, atmospheric circulation patterns) (Kundzewicz et al., 2019), and (ii) are particularly susceptible to the many ongoing anthropogenic changes (Trenberth, 2011). To improve our understanding of the dominant drivers of floods, it becomes fundamental to weigh and explain the temporal attributes of flooding across large scales.

While our current knowledge of the drivers of floods at large spatial and temporal scales has been growing with the increasing availability of historical data and paleoenvironmental proxies (Blöschl et al., 2020; Knox, 2000) together with modern remote sensing information (Alsdorf et al., 2007; C. Huang et al., 2018; Lopez et al., 2020), a comprehensive understanding of the drivers of flooding at the global level is still missing. Indeed, hierarchically bottom-up, causal mechanisms (i.e., processes, such as soil moisture excess after exceeding its infiltration capacity) answering to upper-level drivers have been described from local (Troch et al., 1994; Arora et al., 2021; Alborzi et al., 2022) to catchment (Delgado et al., 2012; Ganguli et al., 2020; Jencso & McGlynn, 2011) and continental levels (Hall et al., 2014; Blöschl et al., 2017; McCabe et al., 2007), yet the larger, global patterns remain underexplored. A mismatch, arising from incongruences in spatial, temporal, and methodological approximations, has been found between the many lines of hydrology research across the planet (Rogger et al., 2017), that constrains the possibilities to upscale from local processes to global patterns (Blöschl, 2006). It might be partly for these reasons that global models still show high uncertainty in anticipating how floods may shift under the conjunct effects of climate change, land cover change, and infrastructure development. A uniform characterization of the timing and extent of floods at the global level and its link with regional drivers is the first step towards the improvement of global flooding modeling.

To this day, global efforts quantifying the temporal dynamics of floods have gone a long way into describing very local (e.g., 900 m^2)- to basin-level variance at different timescales, but have not explored geographical patterns or the drivers to aid their interpretation. Two main lines of research can be distinguished. First, classifications of continental surface water based on remote sensing information have been able to characterize, to different extents, flooding dynamics for a few years (Cao et al., 2014; Prigent et al., 2007) to up to 35 years (Pekel et al., 2016a; Pickens et al., 2020). Their quasi-complete global coverage has allowed the identification of long-term change (over 10 to 35 years) hotspots associated with water infrastructure and climate change effects (Pekel et al., 2016a), and the correlation between rainfall and floods over latitudinal belts (Prigent et al., 2007) and climate regimes (e.g., temperature and precipitation, Cao et al., 2014), among other large-scale questions that can be addressed with these tools. However, neither discuss the existence of geographical patterns of flood timing that could arise from their findings (e.g., across continents, latitudinal and/or longitudinal gradients). Second, recompilations of streamflow records of up to 70 years have given place to detailed classifications of flood season patterns (Do et al., 2020; Lee et al., 2015; B. Merz et al., 2021; Stein et al., 2020), yet the heterogeneous distribution of gauging stations hampers their extrapolation capacity to ungauged catchments and continents (e.g., South America, South Asia, and Africa). Ultimately, global studies have advanced in the classification of floods and the identification of temporal patterns, but their ability to upscale their conclusions on global drivers remains limited due to (i) lack of pattern recognition, (ii) short time periods of observation; and/or (iii) geographically-biased data availability.

In turn, our deepest understanding of large-scale flooding dynamics comes from observations and analyses at single river basins and comparisons across several of them at continental levels. In European river basins, for which long flow records and historical water coverage data are available, short flooding episodes (lasting hours to days) have been linked to precipitation of differing duration as well as snow/thaw episodes (e.g., Blöschl, 2022; Hall & Blöschl, 2018; R. Merz & Blöschl, 2003) and revealed strong interactions with antecedent conditions, e.g., soil moisture (Bertola et al., 2021; Blöschl et al., 2017) (see also Wasko et al., 2020b; Tramblay et al., 2021, for soil moisture relevance in southeastern Australia and Africa, respectively). At the continental level in Europe, complex shifts in flood timing patterns in response to climate change have been documented, including seasonal anticipations in the snowmelt-driven Northeast, delays in storm-led floods around the Mediterranean and North Sea, as well as overall reductions in the South and East and rises the Northwest (Parajka et al., 2010; Blöschl et al., 2017, 2019; Bertola et al., 2021). In North America this was also manifested, as a shortage of the snow accumulating season and consequential earlier onset of thaw and lower spring flood magnitudes have been evidenced for the last thirty years (from weather and gauging stations; Burn & Whitfield, 2016; Cunderlik & Ouarda, 2009; Stewart et al., 2005; Wasko et al., 2020b) (but see also Villarini, 2016). In the flatter tropical setting of the Amazon basin, where floods display slower seasonal timings as explored through remotely sensed information and streamflow records, the effects of rainfall on flooding are strongly mediated by regional water table dynamics (Miguez-Macho & Fan, 2012; Papa et al., 2013). Under drier and (even) flatter settings in Argentina, flood pulses are not linked to well-defined river basins but are associated instead with the expansion and coalescence of isolated surface water bodies connected with rising water table levels (Aragón et al., 2011; Kuppel et al., 2015). Floods in these regions, as well as in southeastern Australia, have shown multiyear fluctuations and have evidenced a high sensitivity to the interactive effects of climate fluctuations and land cover changes across the last thirty years (Tulbure & Broich, 2019; Viglizzo et al., 2011; Whitworth et al., 2012).

When considering the global drivers of flooding at large spatial and temporal scales, it is also important to recognize the overwhelming role of topography over climate driving groundwater depth at the planetary level (Fan et al., 2013). When we increase the observation scale, saturation may progressively gain dominance over infiltration as the flood-generating process (Blöschl, 2022), likely favored by regional topography and shallower water tables (Anyah et al., 2008; Jencso & McGlynn, 2011; Jobbágy et al., 2017). This possible connection between large-scale, slow flooding and topography and its interplay with climate has not been empirically and quantitatively assessed to our knowledge. In this sense, hydrologically-conditioned topography (hereby hydro-topography), based on the average water table depth and associated with the probability of convergence and stagnation of surface water, is one useful parameter to explore the sensitivity of flooding to the most relevant effects of topography.

Here we narrow the definition of timing as the dominating timescale of flood fluctuations (e.g., seasons, years, decades) to evaluate their differing sensitivity to regional drivers. Focusing on slow floods captured by monthly-revisiting sensors onboard satellite platforms (e.g., Landsat), we hypothesize that (1) climate drives the timing of floods through their climatological average rainfall and temperature regimes (e.g., from hot arid to cold humid), (2) topography drives the extent of floods at a regional level, facilitating saturation as the regional average water table level nears the surface, and (3) that the way in which both drivers combine at a given location is a result of their interplay mediated by geographical attributes, especially their latitudinal distribution. As shown, remote sensing provides a unique opportunity to study floods in a consistent way, covering the whole climatic and topographic combination set, and with records going as far back as 1985 for monthly, 30-meter pixels (Pekel et al., 2016a; Pickens et al., 2020). By looking at how floods distribute globally in time and space, by exploring patterns in their timings' similarity, and by comparing their traits across all possible combinations of topography and climate we might be able to provide evidence on how geography controls, offsets, or even intensifies the influence of regional drivers on flood temporal dynamics.

2 Data and methods

2.1 Data selection

To conduct this large-scale study we used Google Earth Engine, an online open processing platform that holds an abundant data catalog of continuous update and provides high-performance cloud computing, allowing researchers to process large amounts of data in next-to-negligible times (Gorelick et al., 2017; Kumar & Mutanga, 2018). Flood extent was estimated through the monthly, 30-meter resolution Global Surface Water Extent dataset v1.3 (GSWE, Pekel et al., 2016a), which is available in Google Earth Engine for the period between 1985-2020. We limited our analysis to 1990-2020 to have three full decades of data, excluding the beginning of the Landsat missions for which there is a limited imagery distribution. Meteorological information (i.e., precipitation and temperature) was derived from TerraClimate, a monthly, 0.04° (~ 5 km at the Equator) gridded dataset available for the 1958-2021 period (Abatzoglou et al., 2018a). Climatic characterization was based on Köppen-Geiger's dominant climate types (Kottek et al., 2006b; Rubel et al., 2017). Topographic characterization was based on the discrete classification by Roebroek et al. (2020), where they integrate the complex effects of local and regional topography on hydrology (therefore, hydro-topography) based on modelled mean water table depth (as per Fan et al., 2013).

To characterize regional slow floods at a global level, we summarized their coverage in a 1-degree rectangular grid, which is an appropriate spatial level to look into regional hydrological processes (covering extensions of hundreds of thousands square km, Blöschl & Sivapalan, 1995), while also matching other relevant remote sensing datasets (e.g., GRACE, Tapley et al., 2004, 2019). We started off with 12,500 cells that exclusively covered continental terrestrial surface, excluding Antarctica. The monthly-level data was pre-processed and aggregated by cell in Google Earth Engine, and extracted to an R environment for further filtering, completion of analyses and plotting (see Data Availability Statement).

2.2 Data filtering and hydrologic year reconstruction

First, we filtered the GSWE dataset according to surface water variation in each 30x30 m pixel between 1990 and 2020. Within the Google Earth Engine platform, and prior to cell-level aggregation, we masked those 30-meter pixels with a coefficient of variation lower than 30%. This threshold proved to satisfactorily exclude lakes and other permanent water bodies across diverse regions (Figure 1). We then aggregated the monthly flooded fraction per 1°x1° cell (i.e., flooded extent) and obtained the regional time series, to which we applied a two-step decision filter to have the best flood-representing time series while acknowledging frequent cloud-induced data gaps. To that end, we (i) excluded months with less than 75% of valid observations, and (ii) excluded cells that had less than 40% qualifiable months over the analyzed period (mainly due to cloud cover). Afterwards, we obtained the month where the flooded extent was at its minimum for each calendar year. The median value across all years was thus set as the start of the hydrologic year. While this is accurate in unimodal surface water dynamics, for bimodal or non-modal (non-uniform) series (see Data Availability Statement) we took the first month that was returned. We also extracted the maxima (peak-occurring months) to associate floods with two main triggers, precipitation and snowmelt.

2.3 Surface water variability and its decomposition

We classified all cells according to the apportionment of temporal variability to (i) seasonal and (ii) interannual fluctuations, and (iii) long-term changes (i.e., net gain or loss over at least 20 years) through a K-means-based, conceptual decision tree. We also sought to further divide the seasonally dominated cells, considering two sub classes based on their association with rainfall and snowmelt, and the long-term class reflecting the direction of change (positive or negative). As a result, we obtained six classes (Figure S1), which summarize the dominant timescale at which flooding fluctuates (e.g, season-level, year-level or decade-level). The equations for the decomposition are explained in this section and exemplified in Figure 2.

After applying quality filters to the monthly time series of 1-degree flood extent, we described each cell through mean, maximum, and minimum extent descriptors, and through two measures of variability: variance (σ^2) and coefficient of variation (CV). Because the temporal data was incomplete, often with large gaps of information, we de-

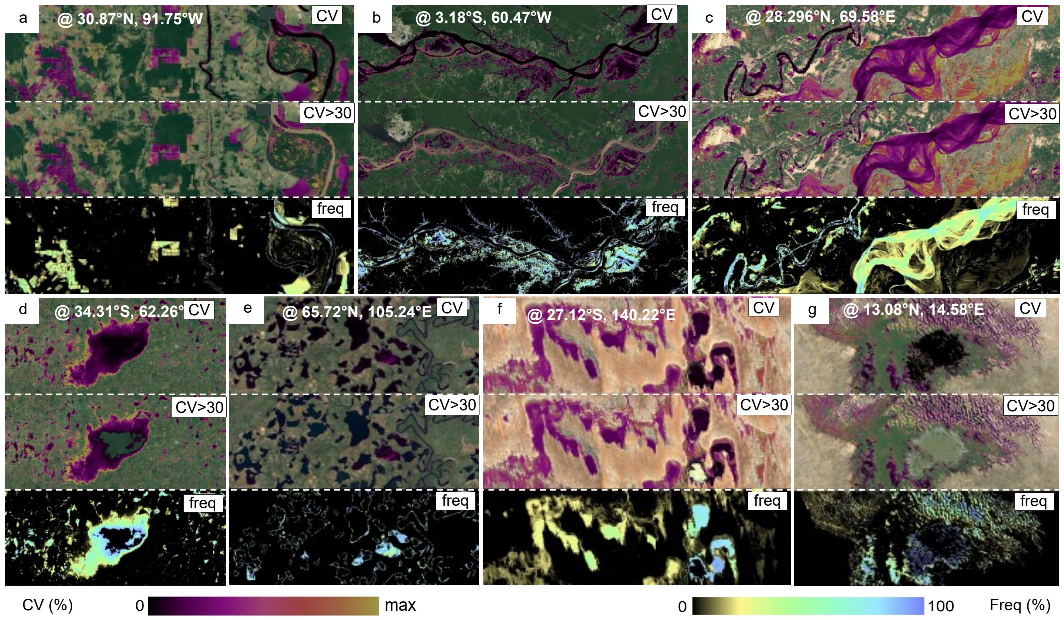

Figure 1. Examples of surface water masking result according to the coefficient of variation of each pixel (threshold = 30%), showing coefficient of variation (top panel), coefficient of variation after masking (central panel) and water cover frequency (bottom panel). (a) Mississippi River, United States; (b) Amazon River, Brazil; (c) Indus River, Pakistan; (d) Picasa Lake, Argentina; (e) glacial lakes in Russia; (f) Coongie Lakes, Australia; (g) Lake Chad, Chad.

cided to apply a simple decomposition based on segmented averages to characterize the variance instead of other approaches (e.g., BFAST; Verbesselt et al., 2010) that require gap-filled time series.

First, we propose that the temporal function of flooded extent (FE) is defined by a combination of cycles or timescales of differing duration, therefore:

$$FE_t = T_t + IA_t + ST_t + r \tag{1}$$

where T_t is the long-term or trend component, which describes a net loss or gain of FE; IA_t is the interannual component that points to year-to-year variations (akin to deseasonalization methods); ST_t is the seasonal component, describing the degree of seasonal fixation (wet season/dry season); and a final error component (r). The function's variance is an additive combination of the variances of each component:

$$\sigma^2{}_{FE} = \sigma^2{}_T + \sigma^2{}_{IA} + \sigma^2{}_{ST} + \sigma^2{}_r \tag{2}$$

To quantify the apportionment of each component (*compweight*), we isolated them and calculated a coefficient of determination, i.e., the fraction of the variance that is explained by them, through:

$$comp\ weight_{\%} = \frac{\sigma^2{}_{comp}}{\sigma^2{}_{FE}} * 100 \tag{3}$$

We explored long-term trends of flood extent through a Mann-Kendall test. If the test was significant ($p<0.001$), a trend slope was derived using the Theil-Sen slope estimator (Sen, 1968; Theil, 1992), which is a common methodology employed in the exploration of trends in hydrology (e.g., Wasko et al., 2020a; Kemter et al., 2023; Blöschl et al., 2017). Then, a long-term series was simulated from the resulting slope coefficient, and its variance was calculated and compared against the FE variance following Eq. (3). It is important to note that long-term trends were only explored in landscapes with at least 20 years of high-quality data, as trends found over shorter periods (e.g., 10 years) might be the result of fluctuations at the year level. Figure S2 locates the "blind spots", i.e., landscapes that did not suffice the minimum timeseries extent according to the filters described in Section 2.2.

The interannual component (IA) corresponds to the effect of hydrologic-yearly means, following the function:

$$IA_t = \begin{cases} FE_y & if\ T = 0 \\ FE_y - T & if\ T \neq 0 \end{cases} \tag{4}$$

where FE_y is the flooded extent averaged for the yth hydrologic year (as defined in the previous section). It should be noted that, if the series had a trend component, part of the interannual component (IA) is explained by the long-term trend. Thus, when a trend was found, the interannual component was calculated as $IA - T$.

We define seasonality as the dynamic that reveals a fix wet and dry season. Even though temporary accumulation of water leads to seasonal floods (i.e., non-permanent), we were further interested in describing how fixed those peaks were. We thus defined seasonality (ST) as the function given by:

$$ST_t = FE_m \tag{5}$$

where FEm is the flooded extent averaged for the mth month.

The error term may be thought of as the fraction of variance that cannot be explained by a single component (i.e., residual variance). This could be due to erratic, non-cyclic fluctuations (at the described timescales) or due to a combination of components that, by themselves, contribute to a small part of the fluctuations (i.e., codominance).

We classified flood timings firstly according to the dominant aspect of its temporal variability through a K-means (Hartigan & Wong, 1979) clustering of four centers, with 500 random initial sets and 1000 iterations. The means of the clusters were interpreted to label each class, and the long-term class was further divided in positive- and negative long-term trend depending on the direction of the LT slope (Figure S1).

2.3.1 Two drivers of seasonality

Seasonal floods can directly result from seasonal precipitation regimes, in which case lags are expected to be short and related to concentration and accumulation times. Yet, they can also be mediated by sub-zero temperatures dictating freezing and thaw cycles, and leading to longer lags and decoupling from precipitation seasonality. We analyzed the temporal proximity of flooding peaks to precipitation peaks as well as to the endings of sub-zero temperature period for all the cells in which the seasonal component was dominant. For this purpose, we calculated lags between precipitation and flooding peaks for each cell and performed bootstrapped simple linear regression, which iterates over thousands of samples resulting from permutations with replacement of the population, to extract the median intercept and slope of peak-to-peak lag relationship. We

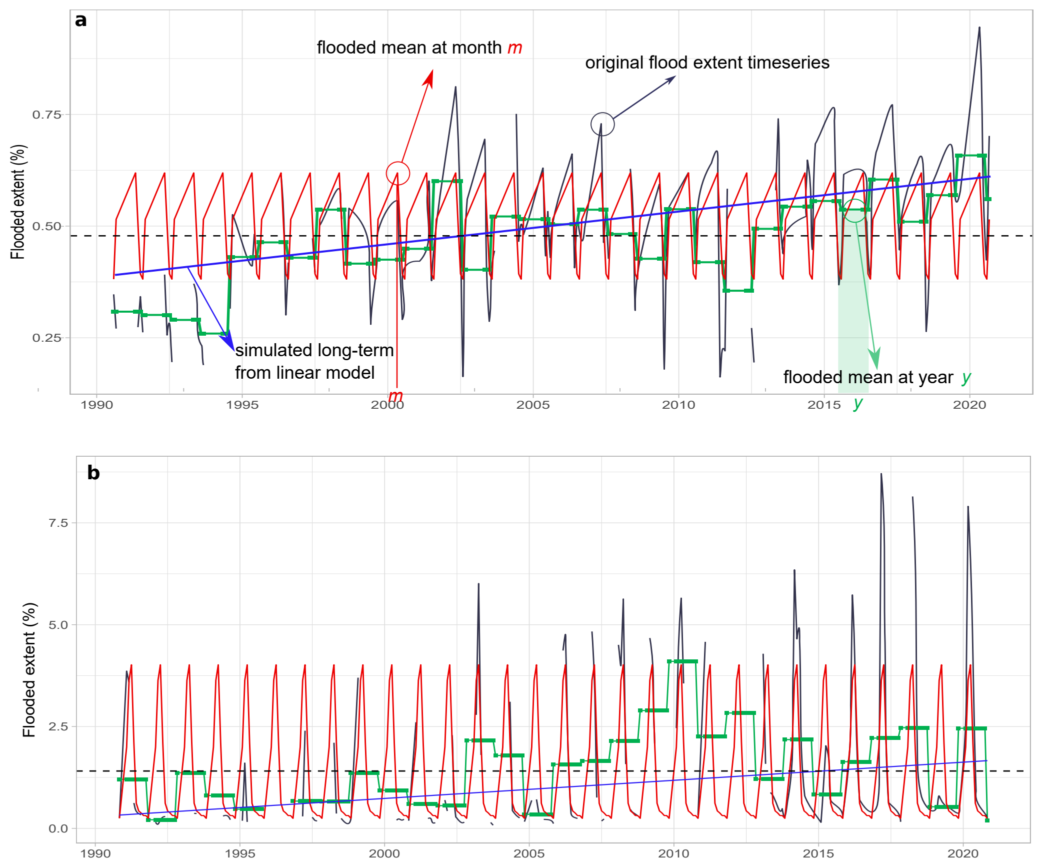

	a	b	c
MFE%	0.48	1.41	3.95
Var	0.024	3.692	8.681
CV%	32	138	75
LT	0.00171	0.00135	*NS*
LT%	23	3	0
IA%	14	16	67
ST%	32	53	7
LT+IA+ST	69	72	74
R%	31	28	26

MFE = mean flooded extent
CV = coefficient of variation
LT = long-term ST = seasonal
IA = interannual R = residual

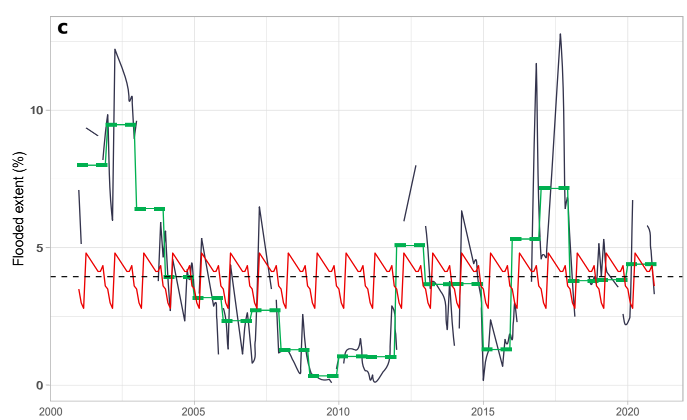

Figure 2. Example of timeseries segmentation into long-term (LT, blue line), interannual (IA, green line) and seasonal (ST, red line) components, with the remaining variance being considered "residual" (R, calculated as 100 minus the sum of LT, IA, and ST relative contributions to the total variance) for three cells: (a) one where there is seasonal and interannual codominance (centered at 52.5°N, 92.5°W), (b) one where seasonality dominates (centered at 15.5°S, 23.5°E), and (c) one where interannual fluctuations dominate (centered at 35.5°S, 62.5°W). The dashed line represents the overall mean flooded extent (MFE).

also included local regression analyses (i.e., LOESS) which generate smoothed regressions along the data, allowing to interpret visually the form of the relationship between the landscape's precipitation and flooding peaks (see Section 2.2). In order to distinguish whether seasonality was driven by rainfall or snowmelt we assumed that a landscape cell had snowmelt effects when it had (a) at least two consecutive months of sub-zero mean temperatures, and (b) a lag of at least four months between precipitation peak and flooding peak. Landscapes that did not follow both criteria were assumed as being directly associated to rainfall. This approach discerned regions with sub-zero winters whose precipitation peaks escape freezing-thawing effects and are closely coupled with floods from those where seasonal flooding cycles are clearly controlled by temperature.

2.4 Flood dynamics across climate and hydro-topography gradients

Last of all, we explored how the observed flooding attributes are associated with climate and to hydro-topography (see Section 2.1). The five climate classes used (A – equatorial, B – arid, C – warm temperate, D – snow/boreal, E – polar) capture the likelihood of water excess generation and of its temporary retention as ice, while the seven classes of hydro-topography (1 – open water and wetland, 2 – lowland, 3 – undulating, 4 – hilly, 5 – low mountainous, 6 – mountainous, 7 – high mountainous) capture a gradient that ranges from high convergence and stagnation to high divergence and drainage that integrate some of the most relevant effects of topography on flooding. We summarized each attribute through a majority value per landscape cell (Figure S3).

3 Results

3.1 Flooding descriptors

Flooded areas display a highly skewed geographical distribution (Figure 3). The mean flooded extent (MFE) of all grid cells averaged 0.48% across all continents excluding Antarctica, with 73.4% of the total flooded area concentrated in the top 20% most flooded grid cells (Figure S4). Slow (long-lasting) floods showed a dominant latitudinal gradient, where northern Eurasia and North America hold the largest share of highly water-covered cells (MFE $>$ 10%) (Figure 3 a). Outside the boreal belt, the valleys of some of the largest rivers and important wetland areas in Africa (Nile, Congo, Niger, and Zambezi rivers), Asia (Ob, Taz, Lena, Indus, Brahmaputra, Ganges, and Yangtze rivers, Poyang Lake), and South America (Amazon, Beni, Paraná, Orinoco and Ucayali rivers, Iberá and Orinoco Llanos wetlands) contributed the next largest number of highly flooded cells.

The overall temporal variability of floods, as captured by the coefficient of variation, revealed a general stable water coverage (CV $<$ 50%, 56.3% of cells) in areas with most flooded area coverage (MFE $>$ 1%) (Figure 3b, S5a), particularly across North America, Amazonia, Europe, and northeastern Asia. Moderate temporal variability (50 $<$ CV $<$ 200 %, 32.5% of cells) took place in all continents and its highest fraction was aggregated in central and southern Argentina, the Sahel and Okavango regions in Africa, central Asia, eastern China, and all across Australia. Lastly, extreme variability (CV $>$ 200%, 11.2% of cells) was found in western and central Australia, northern Sahel, the Saharan desert, the Arabian Peninsula, and Iran.

The decomposition of the variance of flood extent through time showed that seasonal, interannual, and long-term components explained together, on average, 68% of the total variance (more than 90% in the top decile and less than 43% in the lowest decile). Particularly remarkable is the fact that seasonality dominated the variance of 34.1% of the cells, followed by interannual fluctuations (18%) and long-term changes (11.1%). In the rest of the cells (36.7%) more than one timescale of variance prevailed (i.e., interannual and seasonal codominance). The geographic control was evident in the seasonal-to-interannual dominance shift with a distinctive threshold at the -20° latitude (Figure

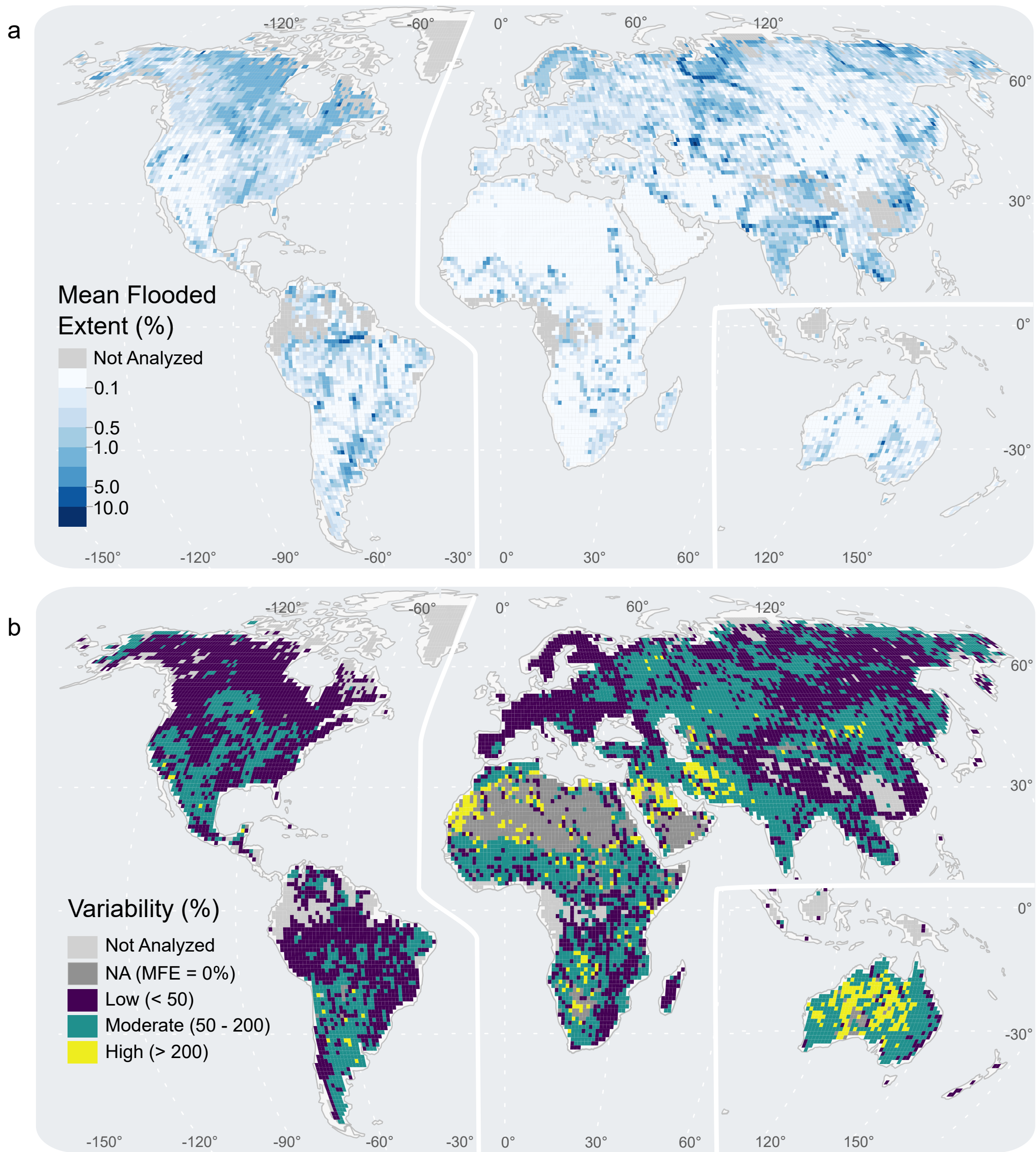

Figure 3. Global distribution of flooding extent (a, mean monthly values) and temporal variability of landscapes with mean flooded extent greater than 0% (b, coefficient of variation). Note that the color scales are nonlinear

4 and Figure S5b). Seasonality dominated flood timings across the northern hemisphere and the tropics, while interannual flooding fluctuations were dominant in northeastern Brazil, Argentina, South Africa, and eastern Australia. Over the United States, a transition from seasonal to interannual dominated flooding fluctuations coincided with the aridity gradient that has its most conspicuous limit along the -97° meridian (Figure S6).

Long-term change (i.e., net gain or loss of flooded area) dominated flooding variability in 11.1% of the cells, with positive trends outweighing negative ones (9.85 and 1.25%, respectively). Positive long-term trends were distributed across all latitudes and were especially important in Europe and central Asia, with magnitudes of up to 1300 km^2 of net flood gain. In contrast, negative long-term trends, which dominated 1.2% of flood timings, were mainly found in mid-latitudinal regions (Figure S5c). Positive long-term dominated dynamics were not as spread nor aggregated as seasonal- and interannual-driven fluctuations, except in China and Canada. Negative change appeared mostly in the Aral Sea, southern Argentina, and central United States (Figure 4, S5c) and may reflect well-documented patterns of increased droughts and irrigation impacts.

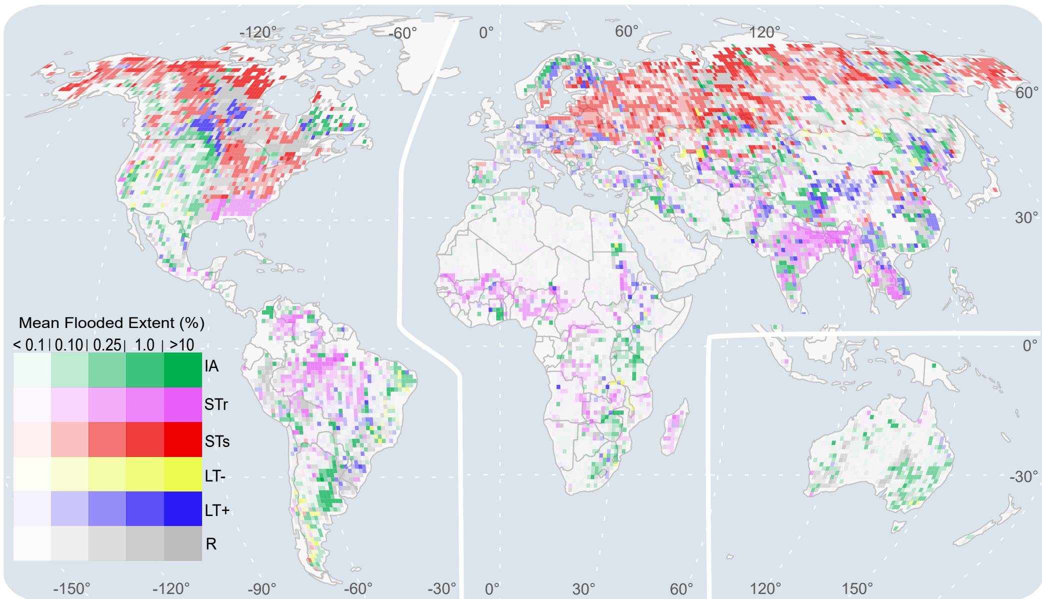

Figure 4. Classification of flood timings according to the major pattern of temporal fluctuation (or lack thereof): interannual (IA, green), rainfall-driven seasonal (ST_r, magenta), snowmelt-driven seasonal (STs, red), negative long-term trend ($LT-$, yellow), positive long-term trend ($LT+$, blue), and residual (R, gray). Color intensity reflects Mean Flooded Extent in a nonlinear scale. It should be noted that a cell might be subject to contributions from more than one timing component (e.g. seasonal with long-term trend), yet the dominant one is highlighted.

3.2 Flooding attributes across climatic and hydro-topographic gradients

Flooding descriptors responded differently to climate and hydro-topography (Figure 5). The magnitude of flooding (as captured by MFE) was mainly explained by hydro-topography, being exponentially biased towards the flattest positions (type 1, open water and wetland, and type 2, lowlands, both characterized by extremely shallow water tables, Figure S3) which had four times more water covered area than the rest of the landscapes, hosting 12% of the flooded areas in just 4.54% of the global land (Figure 5 and Table S1). Outside these hydrologically stagnant cells, undulating to hilly landscapes (types 3 and 4) held 78.17% of global flooded area with a share of 75.88% of global land. These figures dropped for mountainous cells (types 5-7) which hold 9.82% of global flooded area hosting 18.92% of the global land. Climate appeared as a subordinate factor but no less crucial, showing how the Boreal type held the largest share of floods (40% of global flooded area in 24.77% of the global land) and, together with Equatorial type, had more than twice and three times more average flooding than Arid and Temperate types (Figure 5 and Table S1).

Total temporal variability (which had a global average coefficient of variation of 68.4%) peaked towards flat arid landscapes (mean CV = 141%) and decreased towards both more complex and flatter landscapes (Figure 5c). Results showed that hilly and moun-

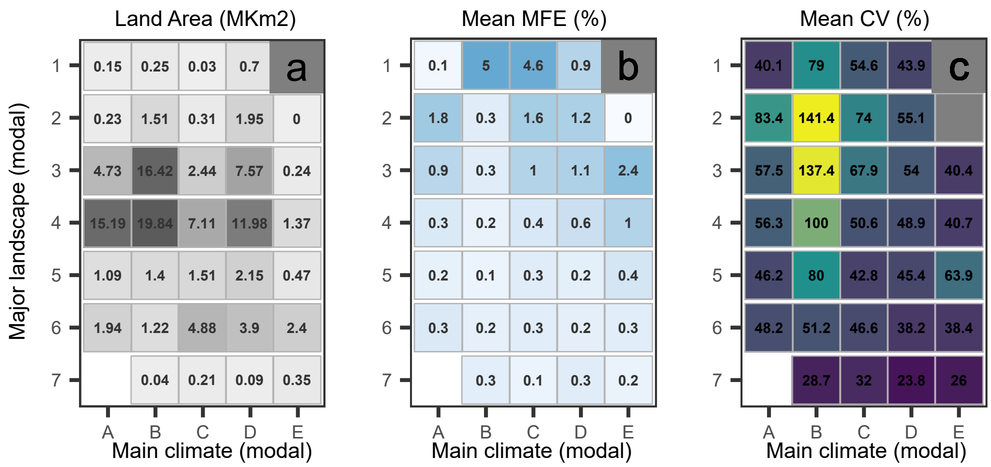

Figure 5. Allocation of flooding temporal descriptors regarding modal main climate (A – equatorial; B – arid; C – warm temperate; D – snow/boreal; E – polar) and modal hydro-topography position (1 – open water and wetland; 2 – lowland; 3 – undulating; 4 – hilly; 5 – low mountainous; 6 – mountainous; 7 – high mountainous). For all 12,500 continental cells (a) total land area (in Mkm^2) per combination, and for the 11,443 analyzed cells: (b) mean MFE (%); (c) mean variability (%). Color scales in panels b-c are reproduced from those in Figure 3 a-b, respectively, which are nonlinear.

tainous cells with low mean water coverage had the most stable floods (mountainous and high mountainous mean CV = 42%). Total variability responded more clearly to climate, being lowest in the Polar climate type (mean CV = 42%) and highest in the Arid type (mean CV = 113%).

As temporal variability was segmented into seasonal, interannual, and long-term components some noticeable patterns emerged (Figure 6). The seasonal component dominated under both Equatorial and Polar climates and gradually yielded its dominance to the interannual component along the Boreal-Temperate-Arid gradient. Interannual variability was prevalent in intermediate hydro-topographies, especially under the Arid and Temperate climates. The positive long-term component of flooding temporal variability was most important in Polar regions, while the negative ones prevailed in Arid regions. Positive trends (most common in mountainous hydro-topographies under all climates) were more widespread than negative ones (most common in flat hydro-topographies with Arid climate).

3.3 Drivers of seasonal flooding

Seasonal fluctuations in flooding may respond to high/low precipitation and/or snow/thaw seasonal cycles, as suggested by the temporal (mis)match between flooding and precipitation peaks throughout the year under different climate types (Figure 7). Varying degrees of synchrony with rainfall seasonality evidenced temperature-mediated lags for flooding growing towards boreal regions after two types of regression analyses. Equatorial and Arid regions revealed the most immediate response of floods to rainfall timing, with a mean lag of 3.5 months, whereas Boreal territories adjusted better instead to the beginning of above-zero temperatures, showing a mean lag of 9.4 months.

Warm regions (climates A, B, and C) had the tightest synchrony between rainfall and flood, with a mean lag of 3.4, 3.7, and 5.2 months, respectively (Figure 7a and c).

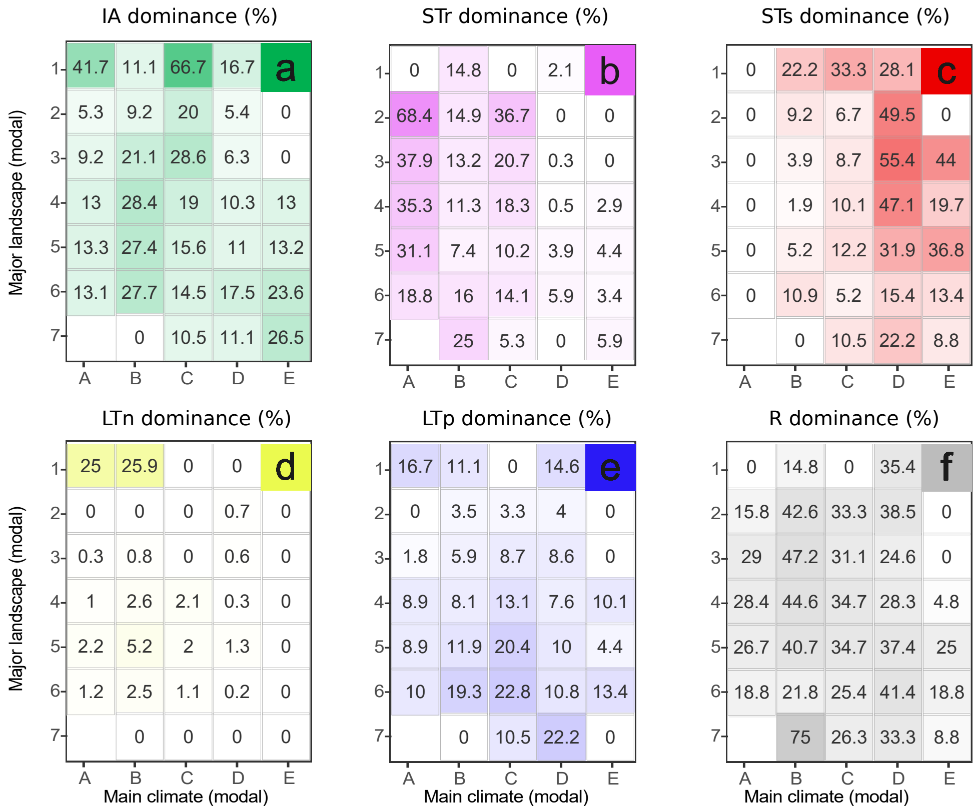

Figure 6. Allocation of flooding temporal descriptors regarding modal main climate (A – equatorial, B – arid, C – warm temperate, D – snow/boreal, E – polar) and modal hydrotopography position (1 – open water and wetland, 2 – lowland, 3 – undulating, 4 – hilly, 5 – low mountainous, 6 – mountainous, 7 – high mountainous). Percentage of cells dominated by (a) interannual, (b) rainfall-driven seasonal, (c) snowmelt-driven seasonal, (d) negative long-term trend, (e) positive long-term trend, (f) residual variance.

Bootstrapped linear regression sustained this association, showing how flooding peak timing was greatly explained by precipitation peak timing for Equatorial climates (intercept = 3.2, slope = 1.05, R^2 = 0.83), while rainfall-driven cells of Arid and Temperate climates presented similar coefficients (intercept = 2.7 and 2.83, slope = 0.98 and 1.07, R^2= 0.58 and 0.7, respectively; Figure S7). Local regression analyses (through a LOESS smoothing function, Figure S8) showed how, for Arid and Temperate climates, an increase of flood-lag in cells where precipitation would peak between May and September while floods peaked between March and May, hinting a decoupled flooding pattern. These were all distributed north of the 30° latitude, where monthly minimum temperatures drop below 0°C in the cold season and could disassociate floods from precipitation (to an up to 10-month lag) independently of the cell's proportion of snow inputs.

In contrast, in the vast fraction of the northern hemisphere registering subzero winter temperatures (climates D and E), seasonal floods occurred mainly where snow precipitation inputs were highest (snow fraction > 30%) and were initiated by the onset of snowmelt between April and June of the following calendar year (Figure 7b, circles). This translates into an up to one month lag to minimum temperature rise above 0°C, and into a great dissociation from precipitation peak (between 8 and 10 months, Figure 7d and S7). Some Polar- and Boreal-dominated cells showed floods closer to precipitation peaks when they occurred earlier in the calendar year. Regression analyses based on bootstrapped linear models reflected this association (intercept = 0.45 and 1.01, R^2 = 0.74 and 0.92, respectively; Figure S7). In these cases, we found that either snow inputs were minor (snow fraction < 30%) and/or that precipitation coupled with the initiation of above-zero temperatures, so the effect of temperature mediating in the translation of rainfall to flood was not as prevalent (Figure 7b and d, triangles).

4 Discussion

Here we present a novel, global characterization of the timing of slow floods. By segmenting monthly time series into short, intermediate, and long timescales of fluctuation we were able to identify and map regions with similar flood timing. Based on this geographic characterization of water coverage patterns we provide evidence about the

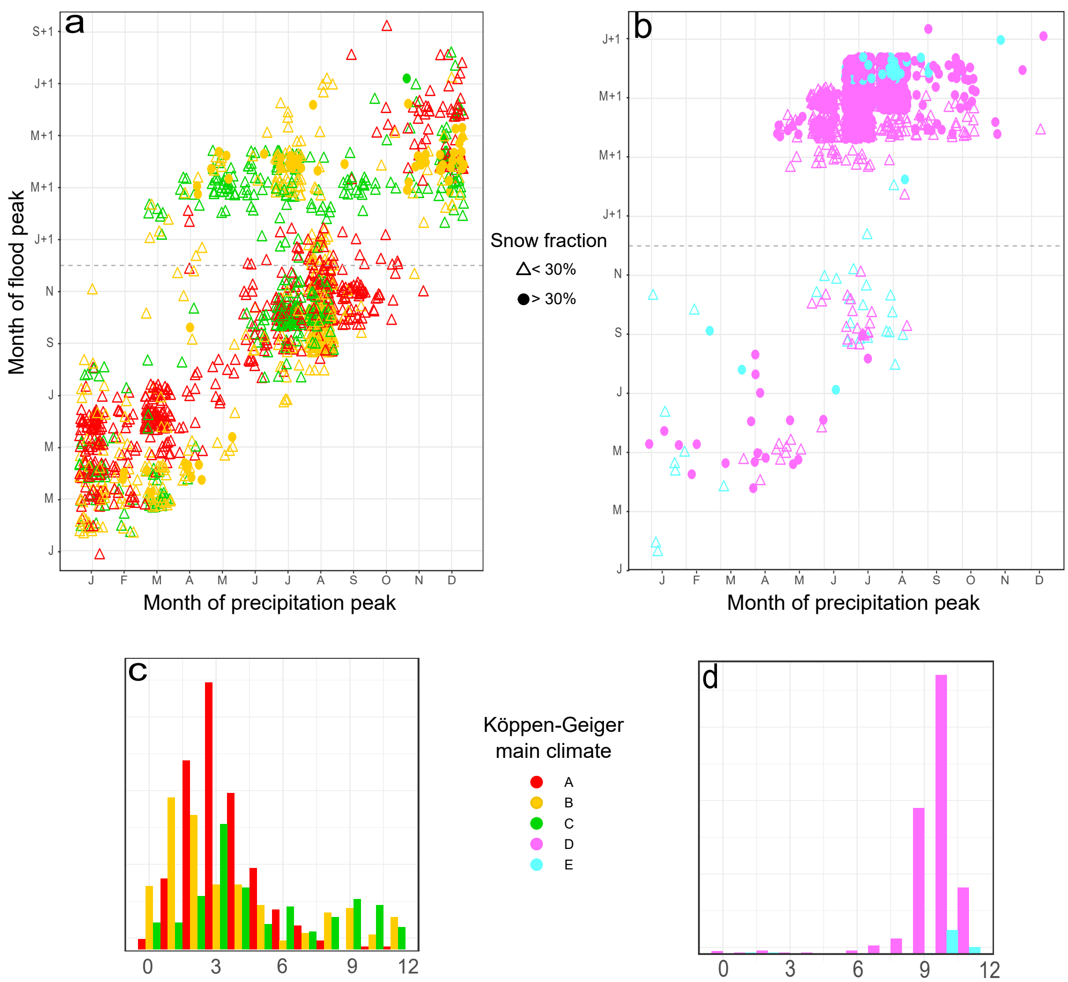

Figure 7. Seasonality of precipitation and floods. Month of flood peak vs. month of precipitation peak for (a) Equatorial (red), warm Temperate (green) and Arid (yellow), and (b) Boreal (purple) and Polar (light blue) Köppen-Geiger climate (KG) dominated cells, differentiating conditions of low (empty triangles) and high snow inputs (circles). Where floods peak on the following calendar year in respect to precipitation, "+1" is indicated. Jitter does not suggest exact dates but is used for a better display of the data. Subplots c) and d) show the precipitation-to-flood peak lag distribution, in months, for each climate type.

large-scale drivers of flooding dynamics, thanks to the exploration of flood attributes across the wide range that regional climate and topography achieve at the global scale. In the first place, we propose how this new geographical perspective of flood timing can aid different global hydrology research avenues. We then focus on the main lessons that it offers about the roles of topography and climate and their interactions driving flooding dynamics. Lastly, we show how these geographical findings provide insight into the differing sensitivities of flooding to global change.

Setting floods in a geographical context allows for exploring patterns influenced by broad environmental gradients including wide latitudinal effects. The distribution of global flood timings, based on the predominant timescale of their fluctuations, revealed that while many highly flooded regions of the world have a predictable flood seasonality, another large fraction experiences floods whose major fluctuations span multiple years. In fact, seasonality dominates flood timing across the boreal and tropical belts, yielding to predominantly interannual timing-dominated fluctuations south of the -20° latitude (Figure 4 and S5). This distinct hemispheric effect could be explained by a lower temperature and precipitation seasonality (i.e. more oceanic climate of the austral temperate belt) which may be overridden by multiyear sources of fluctuations such as ENSO (Kundzewicz et al., 2019; Silva et al., 2017). One important implication of these patterns is that for at least one-fifth of the terrestrial surface, flood analyses should encompass several years to capture the typical span of flooding conditions.

We envision that an explicit global geography of floods, one for which the cartography generated in this study (Figures 3 and 4) is an initial contribution, has two major applications for hydrology research. On one side, it serves as a guide for the synthesis and extrapolation of local studies on flood causes, dynamics, and consequences across regions with similar flood timings. On the other side, it can help select the most appropriate assimilation strategies for land surface models incorporating the currently overlooked effect of flooding on water and energy fluxes, by showing where floods must be accounted for and at what temporal scale their variability should be represented. Several studies have shown how coupling global climate models with land surface models that incorporate surface water dynamics substantially improves the estimation of energy and greenhouse gas fluxes (e.g., Schrapffer et al., 2020; Getirana et al., 2021) as they are key in the energy feedback between the surface and the atmosphere (Houspanossian et al., 2018; Krinner, 2003).

The drivers and process explaining a phenomenon under study depend on the observation scale (O'Neill et al., 1986; Blöschl & Sivapalan, 1995). We conducted our study at a large scale and explored how flood attributes (i.e., mean extent, variability, and timing) respond to regional climatic and topographic constraining drivers. Our analysis demonstrated how high levels of water convergence and groundwater proximity to the surface resulting from regional topography were the main control of surface water accumulation, even after excluding large water reservoirs of low variability (pixels varying less than 30% of the observed period). Landscapes with regional water tables closer than 0.25m (hydrotopographic class 1, mean flooded extent = 1.77%) were two to four times more likely to flood than undulating to hilly regions (mean flooded extent = 0.38 to 0.98%), and ten times more likely to flood than mountains (mean flooded extent = 0.19 to 0.23%) (Figure 5). Fan et al. (2013) estimated that at least 15% of the continental surface water may be in contact with shallow water tables, while several local studies have illustrated the sensitivity of the groundwater-surface contact in that portion of the world to land use and vegetation changes (Cramer & Hobbs, 2002; Favreau et al., 2009; Giménez et al., 2020; Ibrakhimov et al., 2018). Whether the regional mechanism explaining the link between topography, water table, and flooding is dominated by saturation or infiltration processes (Blöschl, 2022) is an attractive question to follow this analysis. For instance, it could be addressed by looking into the shape of the evolving relationship between rainfall, runoff, water table levels and flooded extent (e.g., Gelmini et al., 2022; Reager et al., 2014; Zuecco et al., 2016) at a regional level.

Climate was more important than topography in explaining the temporal variability of floods and their timing. Predictable, seasonally-dominated fluctuations in cold regions gave place to interannual and mixed patterns in temperate climates, and to more irregular and unpredictable patterns in arid regions (Figures 5 and 6). The link between climate, flood peak seasonality, and flood-generating processes has been explored in the contiguous United States (Saharia et al., 2017), where the subordinate climate (with vs. without dry season), as well as the geographical context (inland vs. coastal and intermountainous vs. flatland), also helped explain the varying magnitude of the representative peak discharge. We further identified the process triggering regionally seasonal floods (i.e., rainfall vs. snowmelt), finding that freezing/thawing pulses dictated by temperature seasonality rule flood timings in boreal climates (Figure 6). A third flood-generating process that was included within the rainfall trigger is rain-on-snow events, which were in this study located in northwestern United States, and central and eastern Asia, yet can be locally relevant as demonstrated in Europe (R. Merz & Blöschl, 2003; Viglione et al., 2016; B. Merz et al., 2021), United States (McCabe et al., 2007; Stein et al., 2020) and more recently, over the northern polar belt (Cohen et al., 2015).

While our study did not attempt to attribute long-term trends to causal mechanisms or to the effect of temporal changes in each driver (e.g., climate regime shifts or large-scale topographic modifications), it helps hypothesize on the phenomena that may explain their prevalence as the major source of flooding variability across 11% of the terrestrial surface (Figure 4). Some large clusters of long-term flooding variability dominance with prevailing positive trends observed in Europe, central Asia, and northern North America point towards the effects of global warming, as supported by regional field studies (B. Merz et al., 2021; Woldemeskel & Sharma, 2016) and modeling efforts (Meriö et al., 2019; Vormoor et al., 2015); or the interactive effects of global warming and shifting precipitation regimes (Bertola et al., 2021; Song et al., 2014; Viglione et al., 2016; K. Yang et al., 2014; L. Yang et al., 2021). In other regions, land use may be the prevailing driver, for instance in the cluster in north-eastern China, corresponding to the Songnen plain, where paddy rice has expanded over native grasslands over the last thirty years, likely increasing the amount and duration of water coverage (Liu et al., 2009; Wang et al., 2009; Y. Zhang et al., 2019). In contrast, long-term negative trends in flooding were less abundant and more fragmented. The conspicuous case of the Aral Sea, explained mainly by the impacts of irrigation infrastructure (Jin et al., 2017; Micklin, 1988) appears to be accompanied by other situations in which irrigation may play an important role such as the Mendoza-Colorado rivers in Argentina (Rojas et al., 2020).

Surprisingly, vast areas of increasing flooding detected in our study like that in south-central Canada which may be a result of changes in climate interacting with agricultural practice shifts (Hayashi et al., 2016; J. Huang et al., 2016; Wang & Vivoni, 2022), are poorly explored in the literature. A noticeable aspect of this flood-gaining region is its location in the transition from seasonal-dominated to interannual-dominated flood timings (Figure 4). We speculate that flooding shifts there could be associated with a regime switch from a more regular temperature control to a more variable precipitation control of flood timing (see Chegwidden et al., 2020; Wang & Vivoni, 2022; S. Zhang et al., 2022). In Patagonia, we detected a less-aggregated, negatively-trended cluster which is alarming given the increasing susceptibility to drying of lakes in semi-arid regions. There has been recent evidence generated that indicates how the shallow Colhué Huapi Lake in central Patagonia might be following the Aral Sea's fate, though it is unclear whether it is related to snowpack depletion, increased extraction for human and livestock consumption, decreased precipitation, or a combination of all (Carabajal & Boy, 2021; Scordo et al., 2018). Thus, a key takeaway from our analysis is that a global framework can actually help connect research lines and generate hypotheses arising from the observed regional patterns.

Lastly, we believe that a continuous update of the geography of floods, as flood datasets expand, will become relevant as it could indicate where and how future flood timings may change in response to the effects of climate change. Furthermore, because intensification of the hydrological cycle giving place to higher interannual variability (Huntington, 2006) could result in detrimental effects on water and food security, more attention should be put into understanding the dynamics of interannual-dominated timings. Over the last 32 years, interannual fluctuations have been dominating floods mostly in the global south (i.e., Argentina, Australia, South America, South Africa, and Botswana) but also across the United States, southern India, and northeastern China. By continuously monitoring the dominant timing of floods at a global level, we could anticipate timing shifts (e.g., seasonal to interannual), especially where they are most likely to occur, i.e., in the temperate and dry climate boundaries.

5 Conclusions

Upscaling and extrapolating our growing body of plot- to basin-level knowledge about the mechanisms, drivers, and impacts of flooding is still challenging. With an explicit representation of the global geography of floods, for which this work is an initial contribution, we can contribute top-down insight into the most salient cross-regional flooding patterns and their likely large-scale drivers. The global distribution and timing of "slow" floods (those lasting at least a few days, in opposition to "flash" floods lasting only hours) captured over the last three decades revealed that flooding extent was strongly dictated by regional topography and its effect on the proximity of the water table to the surface (i.e. hydro-topography), with climate having a secondary role. Low regional areas of water convergence were 2-4 times more likely to flood than flat to hilly regions and 10 times more likely to flood than mountains. Across major climate types, floods were more extensive in landscapes having seasonal sub-zero temperatures than the rest combined, suggesting how freezing/thaw cycles favor pulses of liquid water accumulation beyond any other climatic control. The timing of floods (i.e., the dominant timescale at which flooding fluctuates) was mainly driven by climate with seasonality peaking in both equatorial and polar climates and interannual variability rising along the boreal-temperate-arid gradient, with a clear global North/South hemisphere contrast. The dominance of long-term flooding trends prevailed mainly in the boreal belt ($>50^{\circ}$ latitude), where floods are gradually increasing their coverage. Global patterns of positive and negative long-term flooding trends suggest that anthropogenic climate change may influence flooding where warming accentuates thawing cycles (increasing flooding), eliminates freezing (decreasing flooding), or intensifies interannual precipitation variability. Yet, climate change may have its most salient effect on the timing of floods at all temporal levels from seasonal to long-term. As not only water security but the multiple aspects of ecosystems and societies linked to floods are likely to respond to shifting flooding dynamics, it becomes crucial to keep improving our monitoring strategies and our conceptual models of flood controls. In this sense, this study is an example of how large-scale studies with a uniform global coverage serve as a guide for the synthesis and extrapolation of local-to-continental studies on flood causes, dynamics, and consequences across regions with similar flood timings. The detection of patterns and further comparison of the pathways of flood timing across the planet can give place to hypotheses and novel studies in regions that may have gone unnoticed.

Open Research

Data Availability Statement

This study uses data from multiple sources, the majority being freely available in the Google Earth Engine data catalog (`https://developers.google.com/earth-engine/datasets`). Flood extent is based on the Global Surface Water Extent dataset v1.3 (Pekel et al., 2016b). Meteorological data (precipitation and temperature) is derived from TerraClimate (Abatzoglou et al., 2018b). Köppen Geiger climates were downloaded from `http://koeppen-geiger.vu-wien.ac.at/present.htm`, (Kottek et al., 2006a) and hydrologically-conditioned topography from `http://www.hydroshare.org/resource/38ac7dd90c7d4353bb492604981782f0` (Roebroek, 2020). All timeseries were extracted to an R environment (R Core Team, 2021a) for filtering and completion of analysis, and visualization of results, through the doParallel (Microsoft Corporation & Weston, 2020a), factoExtra (Kassambara & Mundt, 2020), foreach (Microsoft Corporation & Weston, 2020b), ggplot2 (Wickham, 2016), ggpubr (Kassambara, 2020), Kendall (McLeod, 2022), moments (Komsta & Novomestky, 2015), robslopes (Raymaekers, 2022), stats (R Core Team, 2021b), sf (Pebesma, 2018), and tidyr (Wickham, 2021) packages. The exploration of distribution uniformity and modes extraction of flooding and precipitation was carried through the LaplacesDemon R package (Statisticat & LLC., 2021).

The derived flood inundation extent dataset and meteorological data associated with this study, as well as the R codes used for processing, analyzing and plotting in this study can be found at `https://doi.org/10.5281/zenodo.7328786` (Torre Zaffaroni et al., 2022).

Acknowledgments

This work was funded by a doctoral scholarship from the National Scientific and Technical Research Council (CONICET) and by the GovernAgua project granted by the Inter American Institute for Global Change Research (IAI SGP-HW 056). The authors declare no conflicts of interest relevant to this study. We thank the three anonymous reviewers for their constructive comments and suggestions which have made our article more compelling. We extend our thanks to S. Aguiar, P. Baldassini, G. Camba Sans, H. Dieguez, and L. Staiano for their valuable comments throughout the stages of the analysis.

References

Abatzoglou, J. T., Dobrowski, S. Z., Parks, S. A., & Hegewisch, K. C. (2018a). TerraClimate, a high-resolution global dataset of monthly climate and climatic water balance from 1958–2015. *Scientific Data*, *5*(1), 170191. doi: 10.1038/sdata.2017.191

Abatzoglou, J. T., Dobrowski, S. Z., Parks, S. A., & Hegewisch, K. C. (2018b). *Terraclimate: Monthly climate and climatic water balance for global terrestrial surfaces, university of idaho* [dataset]. Retrieved from `https://developers.google.com/earth-engine/datasets/catalog/IDAHO_EPSCOR_TERRACLIMATE` doi: 10.1038/sdata.2017.191

Alborzi, A., Zhao, Y., Nazemi, A., Mirchi, A., Mallakpour, I., Moftakhari, H., ... AghaKouchak, A. (2022). The tale of three floods: From extreme events and cascades of highs to anthropogenic floods. *Weather and Climate Extremes*, *38*, 100495. doi: 10.1016/j.wace.2022.100495

Alsdorf, D. E., Rodríguez, E., & Lettenmaier, D. P. (2007). Measuring surface water from space. *Reviews of Geophysics*, *45*(2). doi: 10.1029/2006RG000197

Anyah, R. O., Weaver, C. P., Miguez-Macho, G., Fan, Y., & Robock, A. (2008). Incorporating water table dynamics in climate modeling: 3. Simulated groundwater influence on coupled land-atmosphere variability. *Journal of Geophysical Research Atmospheres*, *113*(7). doi: 10.1029/2007JD009087

Aragón, R., Jobbágy, E. G., & Viglizzo, E. F. (2011). Surface and groundwater dynamics in the sedimentary plains of the Western Pampas (Argentina). *Ecohydrology*, *4*(3), 433–447. doi: 10.1002/eco.149

Arora, A., Pandey, M., Siddiqui, M. A., Hong, H., & Mishra, V. N. (2021). Spatial flood susceptibility prediction in Middle Ganga Plain: comparison of frequency ratio and Shannon's entropy models. *Geocarto International*, *36*(18), 2085–2116. doi: 10.1080/10106049.2019.1687594

Aufdenkampe, A. K., Mayorga, E., Raymond, P. A., Melack, J. M., Doney, S. C., Alin, S. R., ... Yoo, K. (2011). Riverine coupling of biogeochemical cycles between land, oceans, and atmosphere. *Frontiers in Ecology and the Environment*, *9*(1), 53–60. doi: 10.1890/100014

Bertola, M., Viglione, A., Vorogushyn, S., Lun, D., Merz, B., & Blöschl, G. (2021). Do small and large floods have the same drivers of change? A regional attribution analysis in Europe. *Hydrology and Earth System Sciences*, *25*(3), 1347–1364. doi: 10.5194/hess-25-1347-2021

Blöschl, G. (2006). Hydrologic synthesis: Across processes, places, and scales. *Water Resources Research*, *42*(3). doi: 10.1029/2005WR004319

Blöschl, G. (2022). *Flood generation: Process patterns from the raindrop to the ocean* (Vol. 26) (No. 9). Copernicus GmbH. doi: 10.5194/hess-26-2469-2022

Blöschl, G., Hall, J., Parajka, J., Perdigão, R. A. P., Merz, B., Arheimer, B., ... Živković, N. (2017). Changing climate shifts timing of European floods. *Science*, *357*(6351), 588–590. doi: 10.1126/science.aan2506

Blöschl, G., Hall, J., Viglione, A., Perdigão, R. A., Parajka, J., Merz, B., ... Živković, N. (2019). Changing climate both increases and decreases European river floods. *Nature*, *573*(7772), 108–111. doi: 10.1038/s41586-019-1495-6

Blöschl, G., Kiss, A., Viglione, A., Barriendos, M., Böhm, O., Brázdil, R., ... Wetter, O. (2020). Current European flood-rich period exceptional compared with past 500 years. *Nature*, *583*(7817), 560–566. doi: 10.1038/s41586-020-2478-3

Blöschl, G., & Sivapalan, M. (1995). Scale issues in hydrological modelling: A review. *Hydrological Processes*, *9*(3-4), 251–290. doi: 10.1002/hyp.3360090305

Burn, D. H., & Whitfield, P. H. (2016). Changes in floods and flood regimes in Canada. *Canadian Water Resources Journal / Revue canadienne des ressources hydriques*, *41*(1-2), 139–150. doi: 10.1080/07011784.2015.1026844

Cao, X., Chen, J., Chen, L. J., Liao, A. P., Sun, F. D., Li, Y., ... Peng, S. (2014). Preliminary analysis of spatiotemporal pattern of global land surface water. *Science China Earth Sciences*, *57*(10), 2330–2339. doi: 10.1007/s11430-014-4929-x

Carabajal, C. C., & Boy, J. P. (2021). Lake and reservoir volume variations in South America from radar altimetry, ICESat laser altimetry, and GRACE time-variable gravity. *Advances in Space Research*, *68*(2), 652–671. doi: 10.1016/j.asr.2020.04.022

Chegwidden, O., Rupp, D. E., & Nijssen, B. (2020, aug). Climate change alters flood magnitudes and mechanisms in climatically-diverse headwaters across the northwestern United States. *Environmental Research Letters*, *15*(9), 094048. Retrieved from `https://iopscience.iop.org/article/10.1088/1748-9326/ab986fhttps://iopscience.iop.org/article/10.1088/1748-9326/ab986f/meta` doi: 10.1088/1748-9326/AB986F

Cohen, J., Ye, H., & Jones, J. (2015). Trends and variability in rain-on-snow events. *Geophysical Research Letters*, *42*(17), 7115–7122. doi: 10.1002/2015GL065320

Cramer, V. A., & Hobbs, R. J. (2002). Ecological consequences of altered hydrological regimes in fragmented ecosystems in southern Australia: Impacts and possible management responses. *Austral Ecology*, *27*(5), 546–564. doi: 10.1046/j.1442-9993.2002.01215.x

Cunderlik, J. M., & Ouarda, T. B. (2009). Trends in the timing and magnitude of floods in Canada. *Journal of Hydrology*, *375*(3-4), 471–480. doi: 10.1016/j.jhydrol.2009.06.050

Cunderlik, J. M., Ouarda, T. B. M. J., & Bobée, B. (2004). On the objective identification of flood seasons. *Water Resources Research*, *40*(1), 1–12. doi: 10.1029/2003WR002295

Davies, P. M., Bunn, S. E., & Hamilton, S. K. (2008). Primary production in tropical streams and rivers. In *Tropical stream ecology* (pp. 23–42). Academic Press. doi: 10.1016/B978-012088449-0.50004-2

Delgado, J. M., Merz, B., & Apel, H. (2012). A climate-flood link for the lower Mekong River. *Hydrology and Earth System Sciences*, *16*(5), 1533–1541. doi: 10.5194/hess-16-1533-2012

Do, H. X., Westra, S., Leonard, M., & Gudmundsson, L. (2020). Global-Scale Prediction of Flood Timing Using Atmospheric Reanalysis. *Water Resources Research*, *56*(1). doi: 10.1029/2019WR024945

Fan, Y., Li, H., & Miguez-Macho, G. (2013). Global patterns of groundwater table depth. *Science*, *339*(6122), 940–943. doi: 10.1126/science.1229881

Favreau, G., Cappelaere, B., Massuel, S., Leblanc, M., Boucher, M., Boulain, N., & Leduc, C. (2009). Land clearing, climate variability, and water resources increase in semiarid southwest Niger: A review. *Water Resources Research*, *45*(7), 1–18. doi: 10.1029/2007WR006785

Faysse, N., Aguilhon, L., Phiboon, K., & Purotaganon, M. (2020). Mainly farming … but what's next? The future of irrigated farms in Thailand. *Journal of Rural Studies*, *73*, 68–76. doi: 10.1016/j.jrurstud.2019.12.002

Ganguli, P., Nandamuri, Y. R., & Chatterjee, C. (2020). Analysis of persistence in the flood timing and the role of catchment wetness on flood generation in a large river basin in India. *Theoretical and Applied Climatology*, *139*(1-2), 373–388. doi: 10.1007/s00704-019-02964-z

Gelmini, Y., Zuecco, G., Zaramella, M., Penna, D., & Borga, M. (2022). Hysteresis in streamflow-water table relation provides a new classification system of rainfall-runoff events. *Hydrological Processes*, *36*(9), e14685. doi: 10.1002/hyp.14685

Getirana, A., Kumar, S. V., Konapala, G., & Ndehedehe, C. E. (2021). Impacts of Fully Coupling Land Surface and Flood Models on the Simulation of Large Wetlands' Water Dynamics: The Case of the Inner Niger Delta. *Journal of Advances in Modeling Earth Systems*, *13*(5), e2021MS002463. doi: 10.1029/2021MS002463

Giménez, R., Mercau, J. L., Bert, F. E., Kuppel, S., Baldi, G., Houspanossian, J., … Jobbágy, E. G. (2020). Hydrological and productive impacts of recent land-use and land-cover changes in the semiarid Chaco: Understanding novel water excess in water scarce farmlands. *Ecohydrology*, *13*(8), 0–3. doi: 10.1002/eco.2243

Gorelick, N., Hancher, M., Dixon, M., Ilyushchenko, S., Thau, D., & Moore, R. (2017). Google Earth Engine: Planetary-scale geospatial analysis for everyone. *Remote Sensing of Environment*, *202*, 18–27. doi: 10.1016/j.rse.2017.06.031

Hall, J., Arheimer, B., Borga, M., Brázdil, R., Claps, P., Kiss, A., … Blöschl, G. (2014). Understanding flood regime changes in Europe: A state-of-the-art assessment. *Hydrology and Earth System Sciences*, *18*(7), 2735–2772. doi: 10.5194/hess-18-2735-2014

Hall, J., & Blöschl, G. (2018). Spatial patterns and characteristics of flood seasonality in Europe. *Hydrology and Earth System Sciences*, *22*(7), 3883–3901. doi: 10.5194/hess-22-3883-2018

Hartigan, J. A., & Wong, M. A. (1979). Algorithm AS 136: A K-Means Clustering Algorithm. *Applied Statistics*, *28*(1), 100. doi: 10.2307/2346830

Hayashi, M., van der Kamp, G., & Rosenberry, D. O. (2016). Hydrology of Prairie Wetlands: Understanding the Integrated Surface-Water and Groundwater

Processes. *Wetlands*, *36*(2), 237–254. doi: 10.1007/s13157-016-0797-9

Houspanossian, J., Kuppel, S., Nosetto, M. D., Di Bella, C. M., Oricchio, P., Barrucand, M., ... Jobbágy, E. G. (2018). Long-lasting floods buffer the thermal regime of the Pampas. *Theoretical and Applied Climatology*, *131*(1-2), 111–120. doi: 10.1007/s00704-016-1959-7

Huang, C., Chen, Y., Zhang, S., & Wu, J. (2018). Detecting, Extracting, and Monitoring Surface Water From Space Using Optical Sensors: A Review. *Reviews of Geophysics*, *56*(2), 333–360. doi: 10.1029/2018RG000598

Huang, J., Pavlic, G., Rivera, A., Palombi, D., & Smerdon, B. (2016). Cartographier les variations de stock d'eau souterraine avec GRACE: un cas d'étude en Alberta, Canada. *Hydrogeology Journal*, *24*(7), 1663–1680. doi: 10.1007/s10040-016-1412-0

Huntington, T. G. (2006). Evidence for intensification of the global water cycle: Review and synthesis. *Journal of Hydrology*, *319*(1-4), 83–95. doi: 10.1016/j.jhydrol.2005.07.003

Ibrakhimov, M., Awan, U. K., George, B., & Liaqat, U. W. (2018). Understanding surface water–groundwater interactions for managing large irrigation schemes in the multi-country Fergana valley, Central Asia. *Agricultural Water Management*, *201*, 99–106. doi: 10.1016/j.agwat.2018.01.016

Jardine, T. D., Bond, N. R., Burford, M. A., Kennard, M. J., Ward, D. P., Bayliss, P., ... Bunn, S. E. (2015). Does flood rhythm drive ecosystem responses in tropical riverscapes? *Ecology*, *96*(3), 684–692. doi: 10.1890/14-0991.1

Jencso, K. G., & McGlynn, B. L. (2011). Hierarchical controls on runoff generation: Topographically driven hydrologic connectivity, geology, and vegetation. *Water Resources Research*, *47*(11), 1–16. doi: 10.1029/2011WR010666

Jin, Q., Wei, J., Yang, Z.-L., & Lin, P. (2017). Irrigation-Induced Environmental Changes around the Aral Sea: An Integrated View from Multiple Satellite Observations. *Remote Sensing*, *9*(9), 900. doi: 10.3390/rs9090900

Jobbágy, E. G., Tóth, T., Nosetto, M. D., & Earman, S. (2017). On the Fundamental Causes of High Environmental Alkalinity (pH>9): An Assessment of Its Drivers and Global Distribution. *Land Degradation and Development*, *28*(7), 1973–1981. doi: 10.1002/ldr.2718

Kassambara, A. (2020). *ggpubr: 'ggplot2' based publication ready plots* [software]. Retrieved from `https://CRAN.R-project.org/package=ggpubr` (R package version 0.4.0)

Kassambara, A., & Mundt, F. (2020). *factoextra: Extract and visualize the results of multivariate data analyses* [software]. Retrieved from `https://CRAN.R-project.org/package=factoextra` (R package version 1.0.7)

Kemter, M., Marwan, N., Villarini, G., & Merz, B. (2023, jan). Controls on Flood Trends Across the United States. *Water Resources Research*, e2021WR031673. Retrieved from `https://onlinelibrary.wiley.com/doi/full/10.1029/2021WR031673https://onlinelibrary.wiley.com/doi/abs/10.1029/2021WR031673https://agupubs.onlinelibrary.wiley.com/doi/10.1029/2021WR031673` doi: 10.1029/2021WR031673

Knox, J. C. (2000). Sensitivity of modern and Holocene floods to climate change. In *Quaternary science reviews* (Vol. 19, pp. 439–457). Pergamon. doi: 10.1016/S0277-3791(99)00074-8

Komsta, L., & Novomestky, F. (2015). *moments: Moments, cumulants, skewness, kurtosis and related tests* [software]. Retrieved from `https://CRAN.R-project.org/package=moments` (R package version 0.14)

Kottek, M., Grieser, J., Beck, C., Rudolf, B., & Rubel, F. (2006a). [dataset]. Retrieved from `http://koeppen-geiger.vu-wien.ac.at/present.htm` doi: 10.1127/0941-2948/2006/0130

Kottek, M., Grieser, J., Beck, C., Rudolf, B., & Rubel, F. (2006b). World Map of the Köppen-Geiger climate classification updated. *Meteorologische Zeitschrift*,

15(3), 259–263. doi: 10.1127/0941-2948/2006/0130
Krinner, G. (2003). Impact of lakes and wetlands on boreal climate. *Journal of Geophysical Research: Atmospheres*, *108*(16), 4520. doi: 10.1029/2002jd002597
Kumar, L., & Mutanga, O. (2018). Google Earth Engine Applications Since Inception: Usage, Trends, and Potential. *Remote Sensing*, *10*(10), 1509. doi: 10.3390/rs10101509
Kundzewicz, Z. W., Szwed, & Pińskwar. (2019). Climate Variability and Floods—A global Review. *Water*, *11*(7), 1399. doi: 10.3390/w11071399
Kuppel, S., Houspanossian, J., Nosetto, M. D., & Jobbágy, E. G. (2015). What does it take to flood the Pampas?: Lessons from a decade of strong hydrological fluctuations. *Water Resources Research*, *51*(4), 2937–2950. doi: 10.1002/2015WR016966
Lee, D., Ward, P., & Block, P. (2015). Defining high-flow seasons using temporal streamflow patterns from a global model. *Hydrology and Earth System Sciences*, *19*(11), 4689–4705. doi: 10.5194/hess-19-4689-2015
Liu, D., Wang, Z., Song, K., Zhang, B., Hu, L., Huang, N., ... Jiang, G. (2009). Land use/cover changes and environmental consequences in Songnen Plain, Northeast China. *Chinese Geographical Science*, *19*(4), 299–305. doi: 10.1007/s11769-009-0299-2
Loarie, S. R., Lobell, D. B., Asner, G. P., & Field, C. B. (2011). Land-Cover and Surface Water Change Drive Large Albedo Increases in South America*. *Earth Interactions*, *15*(7), 1–16. doi: 10.1175/2010EI342.1
Lopez, T., Al Bitar, A., Biancamaria, S., Güntner, A., & Jäggi, A. (2020). *On the Use of Satellite Remote Sensing to Detect Floods and Droughts at Large Scales* (Vol. 41) (No. 6). Springer. doi: 10.1007/s10712-020-09618-0
McCabe, G. J., Clark, M. P., & Hay, L. E. (2007). Rain-on-snow events in the western United States. *Bulletin of the American Meteorological Society*, *88*(3), 319–328. doi: 10.1175/BAMS-88-3-319
McLeod, A. (2022). *Kendall: Kendall rank correlation and mann-kendall trend test* [software]. Retrieved from `https://CRAN.R-project.org/package=Kendall` (R package version 2.2.1)
Meriö, L., Ala-aho, P., Linjama, J., Hjort, J., Kløve, B., & Marttila, H. (2019). Snow to Precipitation Ratio Controls Catchment Storage and Summer Flows in Boreal Headwater Catchments. *Water Resources Research*, 2018WR023031. doi: 10.1029/2018WR023031
Merz, B., Blöschl, G., Vorogushyn, S., Dottori, F., Aerts, J. C., Bates, P., ... Macdonald, E. (2021). *Causes, impacts and patterns of disastrous river floods* (Vol. 2) (No. 9). Nature Publishing Group. doi: 10.1038/s43017-021-00195-3
Merz, R., & Blöschl, G. (2003). A process typology of regional floods. *Water Resources Research*, *39*(12), 1340. doi: 10.1029/2002WR001952
Micklin, P. (1988). Desiccation of the Aral Sea: A Water Management Disaster in the Soviet Union. *Science*, *241*, 1170–76.
Microsoft Corporation, & Weston, S. (2020a). *doparallel: Foreach parallel adaptor for the 'parallel' package* [software]. Retrieved from `https://CRAN.R-project.org/package=doParallel` (R package version 1.0.16)
Microsoft Corporation, & Weston, S. (2020b). *foreach: Provides foreach looping construct* [software]. Retrieved from `https://CRAN.R-project.org/package=foreach` (R package version 1.5.1)
Miguez-Macho, G., & Fan, Y. (2012). The role of groundwater in the Amazon water cycle: 1. Influence on seasonal streamflow, flooding and wetlands. *Journal of Geophysical Research: Atmospheres*, *117*(D15), n/a–n/a. doi: 10.1029/2012JD017539
O'Neill, R. V., Deangelis, D. L., Waide, J. B., Allen, T. F., & Allen, G. E. (1986). *A hierarchical concept of ecosystems.* Princeton University Press.
Papa, F., Frappart, F., Güntner, A., Prigent, C., Aires, F., Getirana, A., & Maurer,

R. (2013). Surface freshwater storage and variability in the Amazon basin from multi-satellite observations, 1993-2007. *Journal of Geophysical Research Atmospheres*, *118*(21), 11951–11965. doi: 10.1002/2013JD020500

Parajka, J., Kohnová, S., Bálint, G., Barbuc, M., Borga, M., Claps, P., ... Blöschl, G. (2010). Seasonal characteristics of flood regimes across the Alpine-Carpathian range. *Journal of Hydrology*, *394*(1-2), 78–89. doi: 10.1016/j.jhydrol.2010.05.015

Pebesma, E. (2018). *Simple Features for R: Standardized Support for Spatial Vector Data* (Vol. 10) (software No. 1). Retrieved from `https://doi.org/10.32614/RJ-2018-009` doi: 10.32614/RJ-2018-009

Pekel, J.-F., Cottam, A., Gorelick, N., & Belward, A. S. (2016a). High-resolution mapping of global surface water and its long-term changes. *Nature*, *540*(7633), 418–422. doi: 10.1038/nature20584

Pekel, J.-F., Cottam, A., Gorelick, N., & Belward, A. S. (2016b). *High-resolution mapping of global surface water and its long-term changes* [dataset]. Nature Publishing Group. Retrieved from `https://developers.google.com/earth-engine/datasets/catalog/JRC_GSW1_4_MonthlyHistory` doi: 10.1038/nature20584

Pickens, A. H., Hansen, M. C., Hancher, M., Stehman, S. V., Tyukavina, A., Potapov, P., ... Sherani, Z. (2020). Mapping and sampling to characterize global inland water dynamics from 1999 to 2018 with full Landsat time-series. *Remote Sensing of Environment*, *243*(December 2019), 111792. doi: 10.1016/j.rse.2020.111792

Prigent, C., Papa, F., Aires, F., Rossow, W. B., & Matthews, E. (2007). Global inundation dynamics inferred from multiple satellite observations, 1993-2000. *Journal of Geophysical Research Atmospheres*, *112*(12), 1993–2000. doi: 10.1029/2006JD007847

R Core Team. (2021a). *R: A language and environment for statistical computing* [software]. Vienna, Austria. Retrieved from `https://www.R-project.org/`

R Core Team. (2021b). *R: A language and environment for statistical computing* [software]. Vienna, Austria. Retrieved from `https://www.R-project.org/`

Raymaekers, J. (2022). *robslopes: Fast algorithms for robust slopes* [software]. Retrieved from `https://CRAN.R-project.org/package=robslopes` (R package version 1.1.2)

Reager, J. T., Thomas, B. F., & Famiglietti, J. S. (2014). River basin flood potential inferred using GRACE gravity observations at several months lead time. *Nature Geoscience*, *7*(8), 588–592. doi: 10.1038/ngeo2203

Robertson, A. I., Bacon, P., & Heagney, G. (2001). The responses of floodplain primary production to flood frequency and timing. *Journal of Applied Ecology*, *38*(1), 126–136. doi: 10.1046/j.1365-2664.2001.00568.x

Roebroek, C. T. J. (2020). *Global distribution of hydrologic controls on forest growth* [dataset]. HydroShare. Retrieved from `https://www.hydroshare.org/resource/38ac7dd90c7d4353bb492604981782f0` doi: https://doi.org/10.4211/hs.38ac7dd90c7d4353bb492604981782f0

Roebroek, C. T. J., Melsen, L. A., Hoek van Dijke, A. J., Fan, Y., & Teuling, A. J. (2020). Global distribution of hydrologic controls on forest growth. *Hydrology and Earth System Sciences*, *24*(9), 4625–4639. doi: 10.5194/hess-24-4625-2020

Rogger, M., Agnoletti, M., Alaoui, A., Bathurst, J. C., Bodner, G., Borga, M., ... Blöschl, G. (2017). *Land use change impacts on floods at the catchment scale: Challenges and opportunities for future research* (Vol. 53) (No. 7). John Wiley & Sons, Ltd. doi: 10.1002/2017WR020723

Rojas, F., Rubio, C., Rizzo, M., Bernabeu, M., Akil, N., & Martín, F. (2020). Land Use and Land Cover in Irrigated Drylands: a Long-Term Analysis of Changes in the Mendoza and Tunuyán River Basins, Argentina (1986–2018). *Applied*

Spatial Analysis and Policy, *13*(4), 875–899. doi: 10.1007/s12061-020-09335-6

Rubel, F., Brugger, K., Haslinger, K., & Auer, I. (2017). The climate of the European Alps: Shift of very high resolution Köppen-Geiger climate zones 1800-2100. *Meteorologische Zeitschrift*, *26*(2), 115–125. doi: 10.1127/metz/2016/0816

Saharia, M., Kirstetter, P. E., Vergara, H., Gourley, J. J., & Hong, Y. (2017). Characterization of floods in the United States. *Journal of Hydrology*, *548*, 524–535. doi: 10.1016/j.jhydrol.2017.03.010

Sanchis, E., Ferrer, M., Torres, A. G., Cambra-López, M., & Calvet, S. (2012). Effect of Water and Straw Management Practices on Methane Emissions from Rice Fields: A Review Through a Meta-Analysis. *Environmental Engineering Science*, *29*(12), 1053–1062. doi: 10.1089/ees.2012.0006

Schrapffer, A., Sörensson, A., Polcher, J., & Fita, L. (2020). Benefits of representing floodplains in a Land Surface Model: Pantanal simulated with ORCHIDEE CMIP6 version. *Climate Dynamics*, *55*(5-6), 1303–1323. doi: 10.1007/s00382-020-05324-0

Scordo, F., Bohn, V. Y., Piccolo, M. C., & Perillo, G. M. (2018). Mapping and monitoring Lakes Intra-Annual variability in semi-arid regions: A case of study in Patagonian Plains (Argentina). *Water (Switzerland)*, *10*(7), 889. doi: 10.3390/w10070889

Sen, P. K. (1968). Estimates of the Regression Coefficient Based on Kendall's Tau. *Journal of the American Statistical Association*, *63*(324), 1379–1389. doi: 10.1080/01621459.1968.10480934

Silva, A. T., Portela, M. M., Naghettini, M., & Fernandes, W. (2017). A Bayesian peaks-over-threshold analysis of floods in the Itajaí-açu River under stationarity and nonstationarity. *Stochastic Environmental Research and Risk Assessment*, *31*(1), 185–204. doi: 10.1007/s00477-015-1184-4

Simões, N. R., Dias, J. D., Leal, C. M., de Souza Magalhães Braghin, L., Lansac-Tôha, F. A., & Bonecker, C. C. (2013). Floods control the influence of environmental gradients on the diversity of zooplankton communities in a neotropical floodplain. *Aquatic Sciences*, *75*(4), 607–617. doi: 10.1007/s00027-013-0304-9

Sivapalan, M. (2005). Pattern, Process and Function: Elements of a Unified Theory of Hydrology at the Catchment Scale. In *Encyclopedia of hydrological sciences.* John Wiley & Sons, Ltd. doi: 10.1002/0470848944.hsa012

Song, C., Huang, B., Richards, K., Ke, L., & Hien Phan, V. (2014). Accelerated lake expansion on the Tibetan Plateau in the 2000s: Induced by glacial melting or other processes? *Water Resources Research*, *50*(4), 3170–3186. doi: 10.1002/2013WR014724

Statisticat, & LLC. (2021). *Laplacesdemon tutorial* [software]. Bayesian-Inference.com. Retrieved from `https://web.archive.org/web/20150206004624/http://www.bayesian-inference.com/software` (R package version 16.1.6)

Stein, L., Pianosi, F., & Woods, R. (2020). Event-based classification for global study of river flood generating processes. *Hydrological Processes*, *34*(7), 1514–1529. doi: 10.1002/hyp.13678

Stewart, I. T., Cayan, D. R., & Dettinger, M. D. (2005). Changes toward earlier streamflow timing across western North America. *Journal of Climate*, *18*(8), 1136–1155. doi: 10.1175/JCLI3321.1

Tapley, B. D., Bettadpur, S., Ries, J. C., Thompson, P. F., & Watkins, M. M. (2004). GRACE Measurements of Mass Variability in the Earth System. *Science*, *305*(5683), 503–505. doi: 10.1126/science.1099192

Tapley, B. D., Watkins, M. M., Flechtner, F., Reigber, C., Bettadpur, S., Rodell, M., … Velicogna, I. (2019). Contributions of GRACE to understanding climate change. *Nature Climate Change*, *9*(5), 358–369. doi: 10.1038/s41558-019-0456-2

Theil, H. (1992). A Rank-Invariant Method of Linear and Polynomial Regression Analysis. In (pp. 345–381). Springer, Dordrecht. doi: 10.1007/978-94-011-2546-8_20

Torre Zaffaroni, P., Baldi, G., Texeira, M., Di Bella, C. M., & Jobbágy, E. G. (2022, jun). *The Timing of Global Floods and its Association with Climate and Topography - associated Data and Codes* [software]. Zenodo. doi: 10.5281/zenodo.7328786

Tramblay, Y., Villarini, G., El Khalki, E. M., Gründemann, G., & Hughes, D. (2021, jun). Evaluation of the Drivers Responsible for Flooding in Africa. *Water Resources Research*, *57*(6), e2021WR029595. Retrieved from `https://onlinelibrary.wiley.com/doi/full/10.1029/2021WR029595https://onlinelibrary.wiley.com/doi/abs/10.1029/2021WR029595https://agupubs.onlinelibrary.wiley.com/doi/10.1029/2021WR029595` doi: 10.1029/2021WR029595

Trenberth, K. E. (2011). Changes in precipitation with climate change. *Climate Research*, *47*(1-2), 123–138. doi: 10.3354/cr00953

Troch, P. A., Smith, J. A., Wood, E. F., & de Troch, F. P. (1994). Hydrologic controls of large floods in a small basin: central Appalachian case study. *Journal of Hydrology*, *156*(1-4), 285–309. doi: 10.1016/0022-1694(94)90082-5

Tulbure, M. G., & Broich, M. (2019). Spatiotemporal patterns and effects of climate and land use on surface water extent dynamics in a dryland region with three decades of Landsat satellite data. *Science of the Total Environment*, *658*, 1574–1585. doi: 10.1016/j.scitotenv.2018.11.390

Verbesselt, J., Hyndman, R., Newnham, G., & Culvenor, D. (2010). Detecting trend and seasonal changes in satellite image time series. *Remote Sensing of Environment*, *114*(1), 106–115. doi: 10.1016/j.rse.2009.08.014

Viglione, A., Merz, B., Viet Dung, N., Parajka, J., Nester, T., & Blöschl, G. (2016). Attribution of regional flood changes based on scaling fingerprints. *Water Resources Research*, *52*(7), 5322–5340. doi: 10.1002/2016WR019036

Viglizzo, E. F., Frank, F. C., Carreño, L. V., Jobbágy, E. G., Pereyra, H., Clatt, J., ... Ricard, M. F. (2011). Ecological and environmental footprint of 50 years of agricultural expansion in Argentina. *Global Change Biology*, *17*(2), 959–973. doi: 10.1111/j.1365-2486.2010.02293.x

Villarini, G. (2016). On the seasonality of flooding across the continental United States. *Advances in Water Resources*, *87*, 80–91. doi: 10.1016/j.advwatres.2015.11.009

Vormoor, K., Lawrence, D., Heistermann, M., & Bronstert, A. (2015). Climate change impacts on the seasonality and generation processes of floods – Projections and uncertainties for catchments with mixed snowmelt/rainfall regimes. *Hydrology and Earth System Sciences*, *19*(2), 913–931. doi: 10.5194/hess-19-913-2015

Wang, Z., Song, K., Zhang, B., Liu, D., Ren, C., Luo, L., ... Liu, Z. (2009). Shrinkage and fragmentation of grasslands in the West Songnen Plain, China. *Agriculture, Ecosystems and Environment*, *129*(1-3), 315–324. doi: 10.1016/j.agee.2008.10.009

Wang, Z., & Vivoni, E. R. (2022). Individualized and Combined Effects of Future Urban Growth and Climate Change on Irrigation Water Use in Central Arizona. *Journal of the American Water Resources Association*, *58*(3), 370–387. doi: 10.1111/1752-1688.13005

Warfe, D. M., Pettit, N. E., Davies, P. M., Pusey, B. J., Hamilton, S. K., Kennard, M. J., ... Halliday, I. A. (2011). *The 'wet-dry' in the wet-dry tropics drives river ecosystem structure and processes in northern Australia* (Vol. 56) (No. 11). John Wiley & Sons, Ltd. doi: 10.1111/j.1365-2427.2011.02660.x

Wasko, C., Nathan, R., & Peel, M. C. (2020a, mar). Changes in Antecedent Soil Moisture Modulate Flood Seasonality in a Changing Climate. *Water Resources*

Research, *56*(3), no. Retrieved from https://onlinelibrary.wiley.com/doi/full/10.1029/2019WR026300https://onlinelibrary.wiley.com/doi/abs/10.1029/2019WR026300https://agupubs.onlinelibrary.wiley.com/doi/10.1029/2019WR026300 doi: 10.1029/2019WR026300

Wasko, C., Nathan, R., & Peel, M. C. (2020b). Trends in Global Flood and Streamflow Timing Based on Local Water Year. *Water Resources Research*, *56*(8), 0–2. doi: 10.1029/2020WR027233

Whitworth, K. L., Baldwin, D. S., & Kerr, J. L. (2012). Drought, floods and water quality: Drivers of a severe hypoxic blackwater event in a major river system (the southern Murray-Darling Basin, Australia). *Journal of Hydrology*, *450-451*, 190–198. Retrieved from http://dx.doi.org/10.1016/j.jhydrol.2012.04.057 doi: 10.1016/j.jhydrol.2012.04.057

Wickham, H. (2016). *ggplot2: Elegant graphics for data analysis* [software]. Springer-Verlag New York. Retrieved from https://ggplot2.tidyverse.org

Wickham, H. (2021). *tidyr: Tidy messy data* [software]. Retrieved from https://CRAN.R-project.org/package=tidyr (R package version 1.1.4)

Woldemeskel, F., & Sharma, A. (2016). Should flood regimes change in a warming climate? The role of antecedent moisture conditions. *Geophysical Research Letters*, *43*(14), 7556–7563. doi: 10.1002/2016GL069448

Yang, K., Wu, H., Qin, J., Lin, C., Tang, W., & Chen, Y. (2014). Recent climate changes over the Tibetan Plateau and their impacts on energy and water cycle: A review. *Global and Planetary Change*, *112*, 79–91. doi: 10.1016/j.gloplacha.2013.12.001

Yang, L., Yang, Y., Villarini, G., Li, X., Hu, H., Wang, L., … Tian, F. (2021). Climate More Important for Chinese Flood Changes Than Reservoirs and Land Use. *Geophysical Research Letters*, *48*(11), e2021GL093061. doi: 10.1029/2021GL093061

Zhang, S., Zhou, L., Zhang, L., Yang, Y., Wei, Z., Zhou, S., … Dai, Y. (2022, nov). Reconciling disagreement on global river flood changes in a warming climate. *Nature Climate Change 2022 12:12*, *12*(12), 1160–1167. Retrieved from https://www.nature.com/articles/s41558-022-01539-7 doi: 10.1038/s41558-022-01539-7

Zhang, Y., Zang, S., Sun, L., Yan, B., Yang, T., Yan, W., … Qi, J. (2019). Characterizing the changing environment of cropland in the Songnen Plain, Northeast China, from 1990 to 2015. *Journal of Geographical Sciences*, *29*(5), 658–674. doi: 10.1007/s11442-019-1620-3

Zuecco, G., Penna, D., Borga, M., & van Meerveld, H. J. (2016). A versatile index to characterize hysteresis between hydrological variables at the runoff event timescale. *Hydrological Processes*, *30*(9), 1449–1466. doi: 10.1002/hyp.10681

Figure 1.

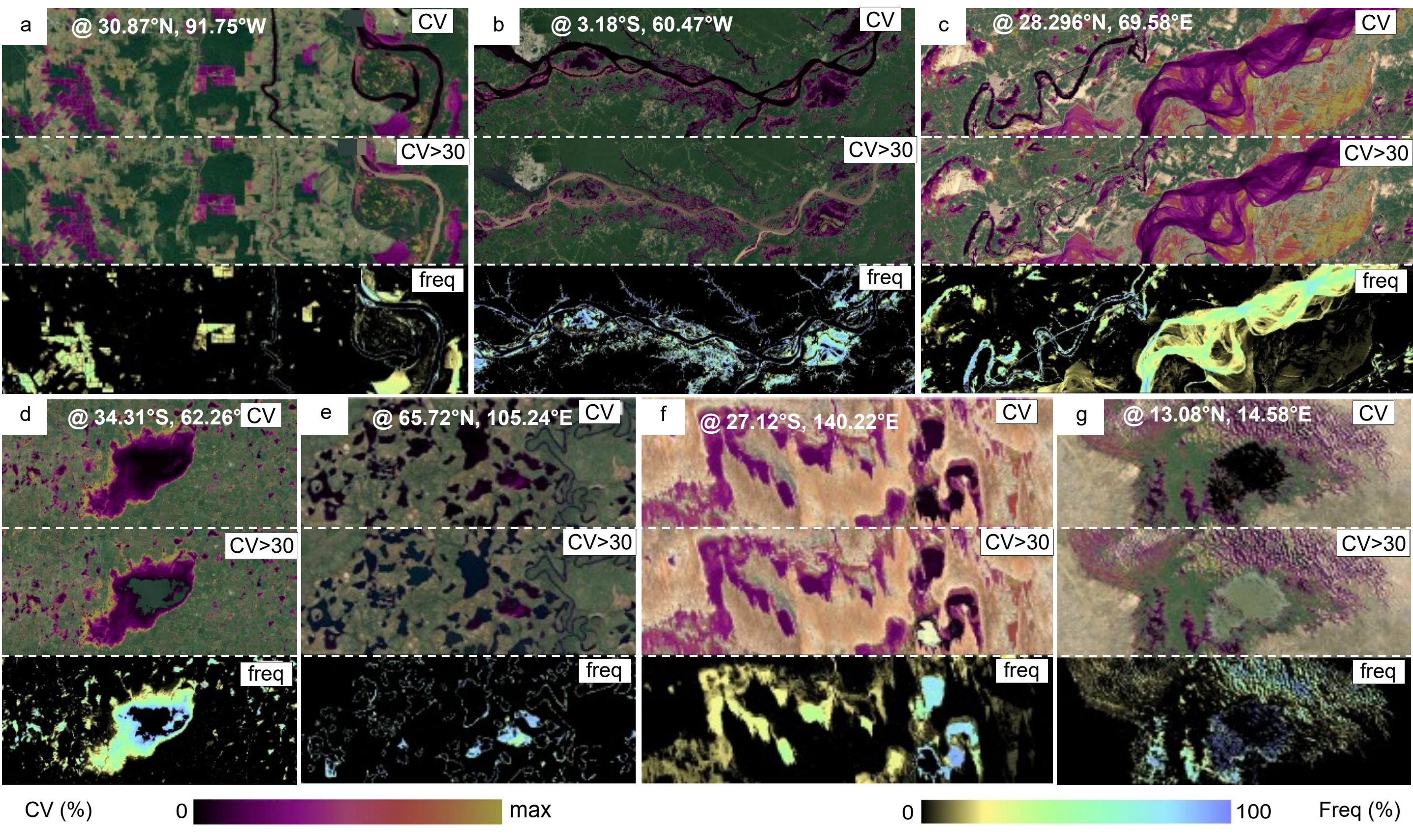
a
@ 30.87°N, 91.75°W
CV
CV>30
freq
b
@ 3.18°S, 60.47°W
CV
CV>30
freq
c
@ 28.296°N, 69.58°E
CV
CV>30
freq
d
@ 34.31°S, 62.26°
CV
CV>30
freq
e
@ 65.72°N, 105.24°E
CV
CV>30
freq
f
@ 27.12°S, 140.22°E
CV
CV>30
freq
g
@ 13.08°N, 14.58°E
CV
CV>30
freq
CV (%)
0
max
0
100
Freq (%)

Figure 2.

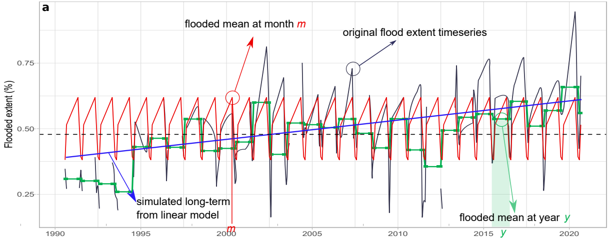

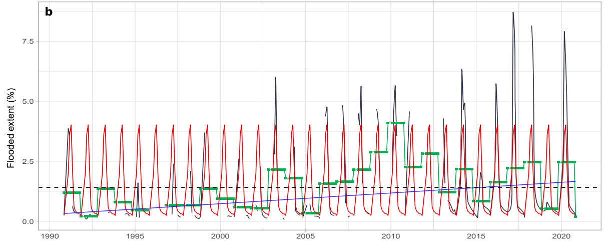

	a	b	c
MFE%	0.48	1.41	3.95
Var	0.024	3.692	8.681
CV%	32	138	75
LT	0.00171	0.00135	*NS*
LT%	23	3	0
IA%	14	16	67
ST%	32	53	7
LT+IA+ST	69	72	74
R%	31	28	26

MFE = mean flooded extent
CV = coefficient of variation
LT = long-term
ST = seasonal
IA = interannual
R = residual

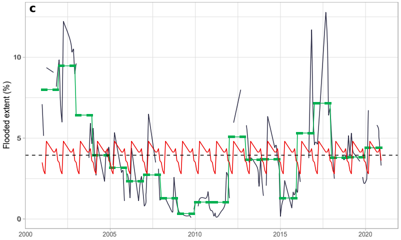

Figure 3.

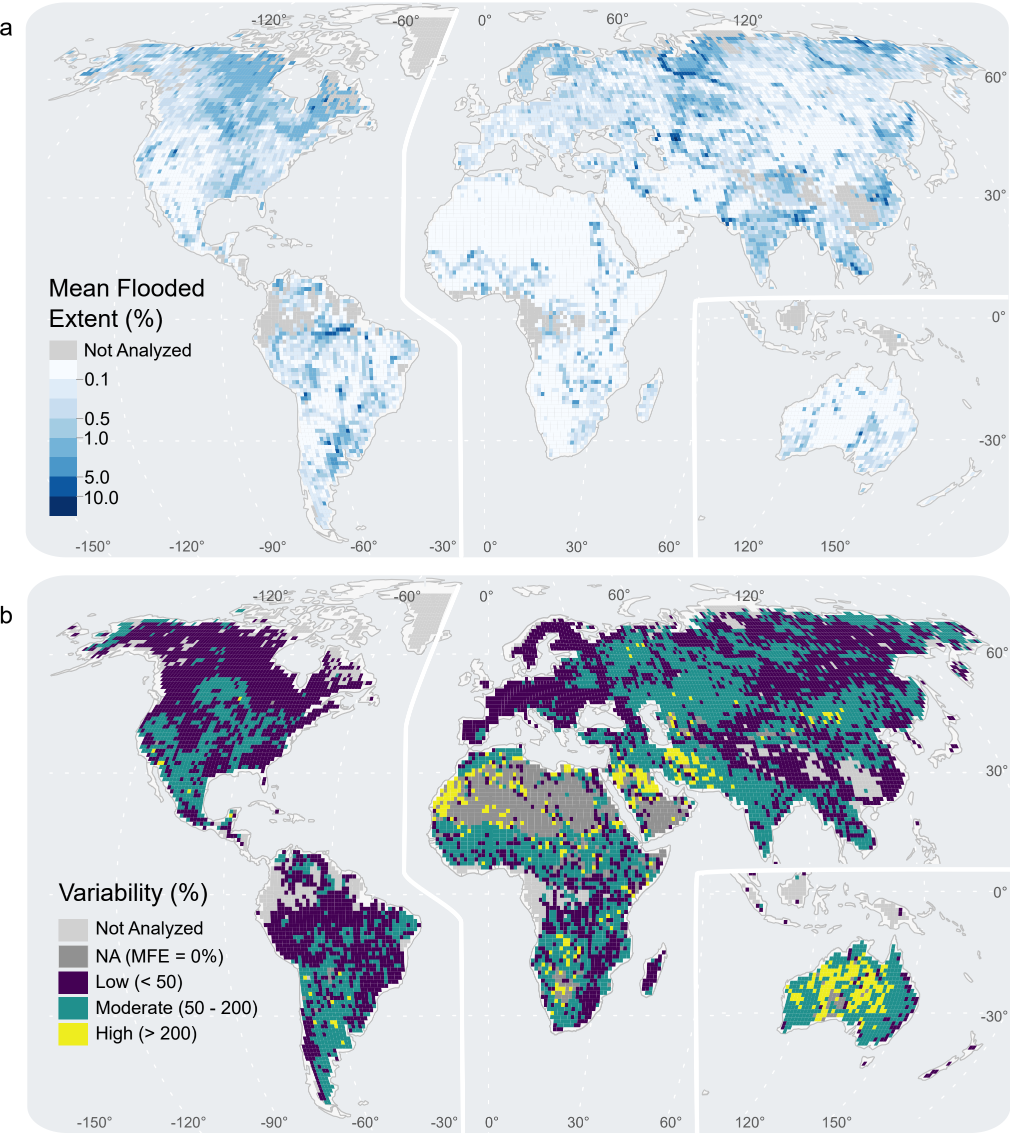

a
Mean Flooded Extent (%)
Not Analyzed
0.1
0.5
1.0
5.0
10.0
b
Variability (%)
Not Analyzed
NA (MFE = 0%)
Low (< 50)
Moderate (50 - 200)
High (> 200)
-150°
-120°
-90°
-60°
-30°
0°
30°
60°
120°
150°

Figure 4.

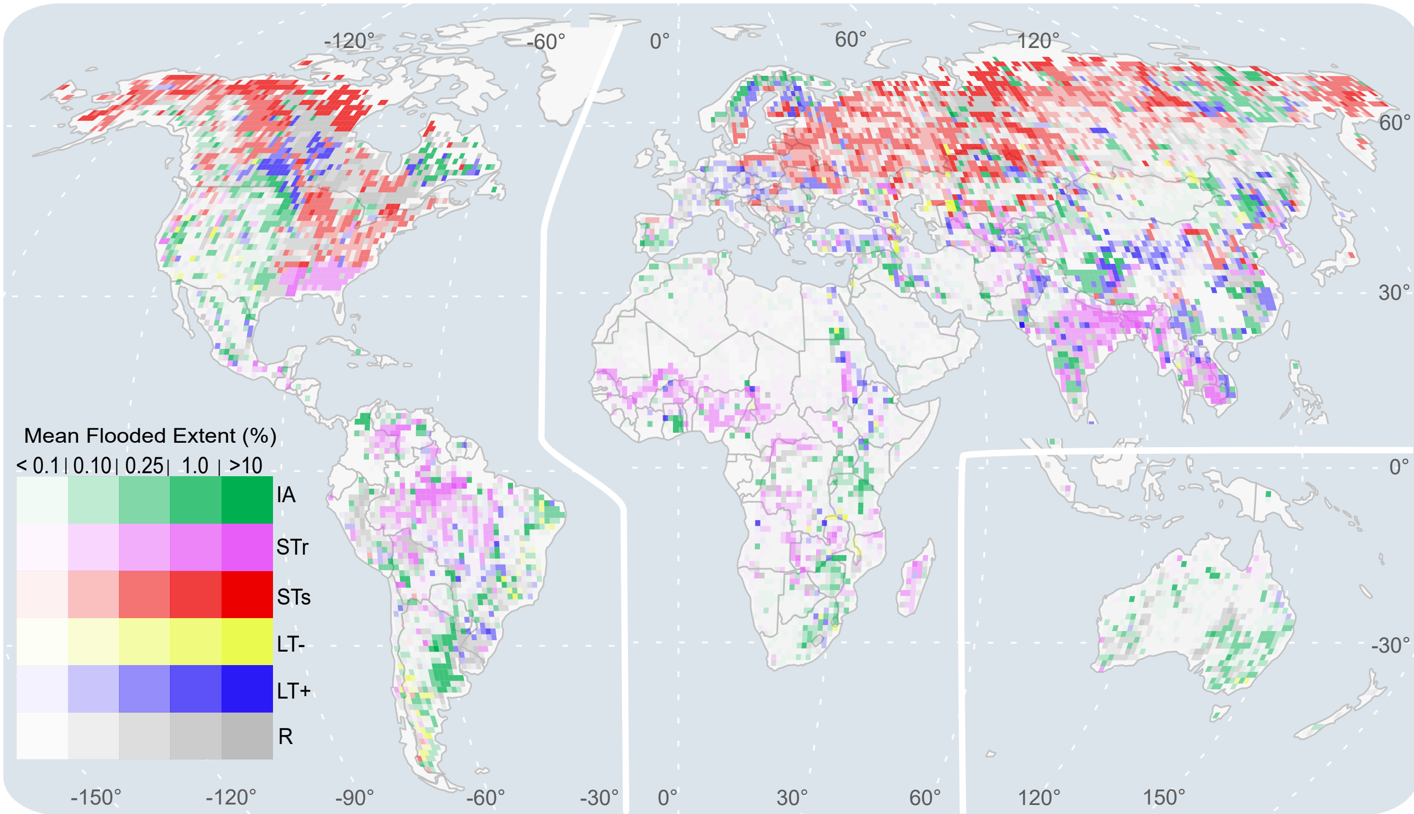

Mean Flooded Extent (%)
< 0.1 | 0.10 | 0.25 | 1.0 | >10
IA
STr
STs
LT-
LT+
R
-120°
-60°
0°
60°
120°
60°
30°
0°
-30°
-150°
-120°
-90°
-60°
-30°
0°
30°
60°
120°
150°

Figure 5.

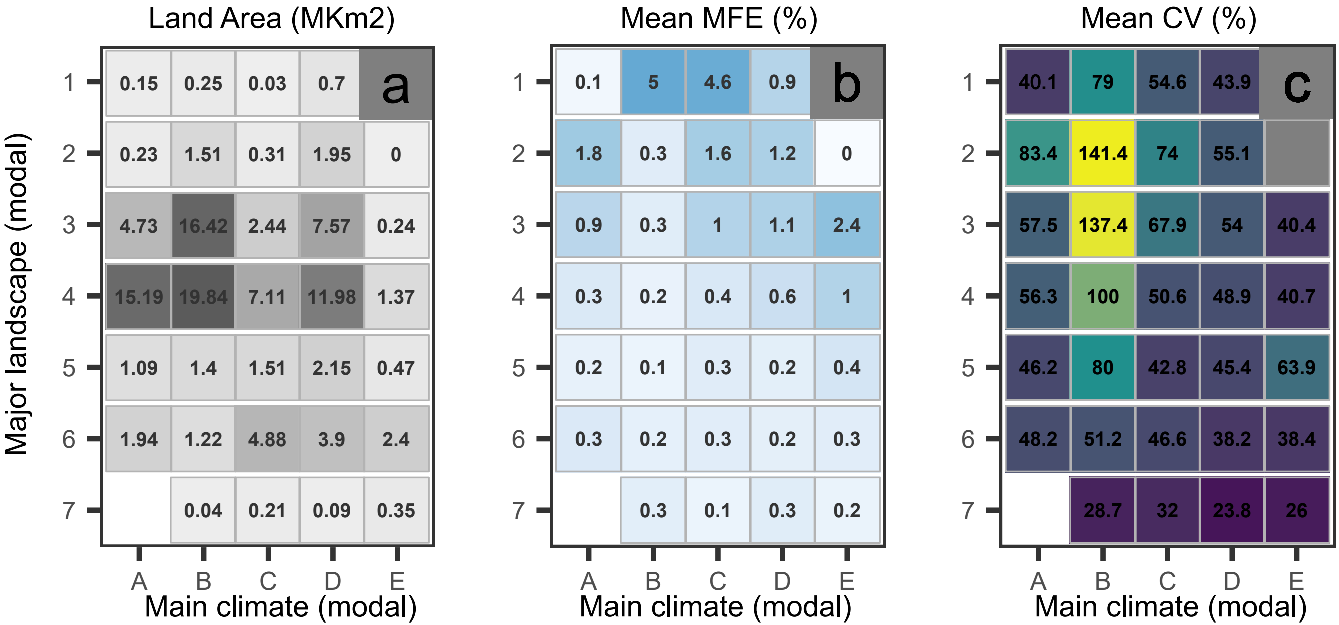
Land Area (MKm2)
Mean MFE (%)
Mean CV (%)
a
b
c
Major landscape (modal)
Main climate (modal)
1
2
3
4
5
6
7
A
B
C
D
E
0.15 0.25 0.03 0.7
0.23 1.51 0.31 1.95 0
4.73 16.42 2.44 7.57 0.24
15.19 19.84 7.11 11.98 1.37
1.09 1.4 1.51 2.15 0.47
1.94 1.22 4.88 3.9 2.4
0.04 0.21 0.09 0.35
0.1 5 4.6 0.9
1.8 0.3 1.6 1.2 0
0.9 0.3 1 1.1 2.4
0.3 0.2 0.4 0.6 1
0.2 0.1 0.3 0.2 0.4
0.3 0.2 0.3 0.2 0.3
0.3 0.1 0.3 0.2
40.1 79 54.6 43.9
83.4 141.4 74 55.1
57.5 137.4 67.9 54 40.4
56.3 100 50.6 48.9 40.7
46.2 80 42.8 45.4 63.9
48.2 51.2 46.6 38.2 38.4
28.7 32 23.8 26

Figure 6.

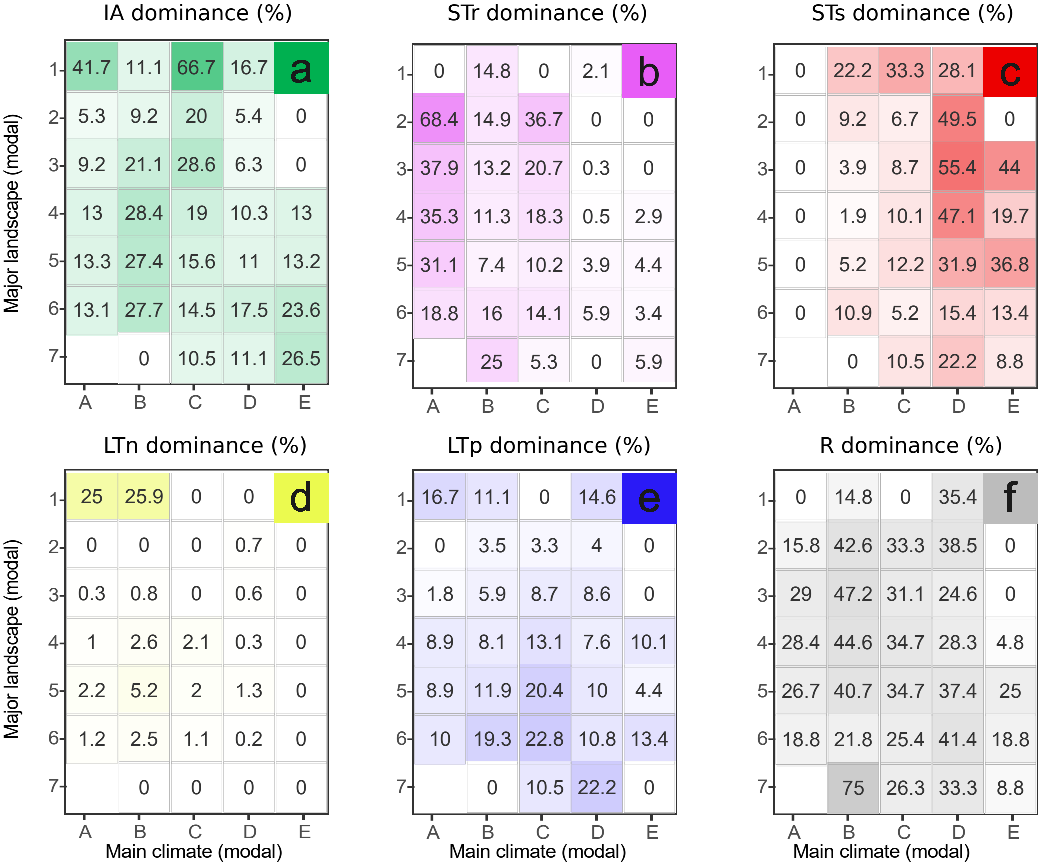
IA dominance (%)
STr dominance (%)
STs dominance (%)
LTn dominance (%)
LTp dominance (%)
R dominance (%)
a
b
c
d
e
f
Major landscape (modal)
Main climate (modal)
A B C D E
1 2 3 4 5 6 7
41.7 11.1 66.7 16.7
5.3 9.2 20 5.4 0
9.2 21.1 28.6 6.3 0
13 28.4 19 10.3 13
13.3 27.4 15.6 11 13.2
13.1 27.7 14.5 17.5 23.6
0 10.5 11.1 26.5
0 14.8 0 2.1
68.4 14.9 36.7 0 0
37.9 13.2 20.7 0.3 0
35.3 11.3 18.3 0.5 2.9
31.1 7.4 10.2 3.9 4.4
18.8 16 14.1 5.9 3.4
25 5.3 0 5.9
0 22.2 33.3 28.1
0 9.2 6.7 49.5 0
0 3.9 8.7 55.4 44
0 1.9 10.1 47.1 19.7
0 5.2 12.2 31.9 36.8
0 10.9 5.2 15.4 13.4
0 10.5 22.2 8.8
25 25.9 0 0
0 0 0 0.7 0
0.3 0.8 0 0.6 0
1 2.6 2.1 0.3 0
2.2 5.2 2 1.3 0
1.2 2.5 1.1 0.2 0
0 0 0 0
16.7 11.1 0 14.6
0 3.5 3.3 4 0
1.8 5.9 8.7 8.6 0
8.9 8.1 13.1 7.6 10.1
8.9 11.9 20.4 10 4.4
10 19.3 22.8 10.8 13.4
0 10.5 22.2 0
0 14.8 0 35.4
15.8 42.6 33.3 38.5 0
29 47.2 31.1 24.6 0
28.4 44.6 34.7 28.3 4.8
26.7 40.7 34.7 37.4 25
18.8 21.8 25.4 41.4 18.8
75 26.3 33.3 8.8

Figure 7.

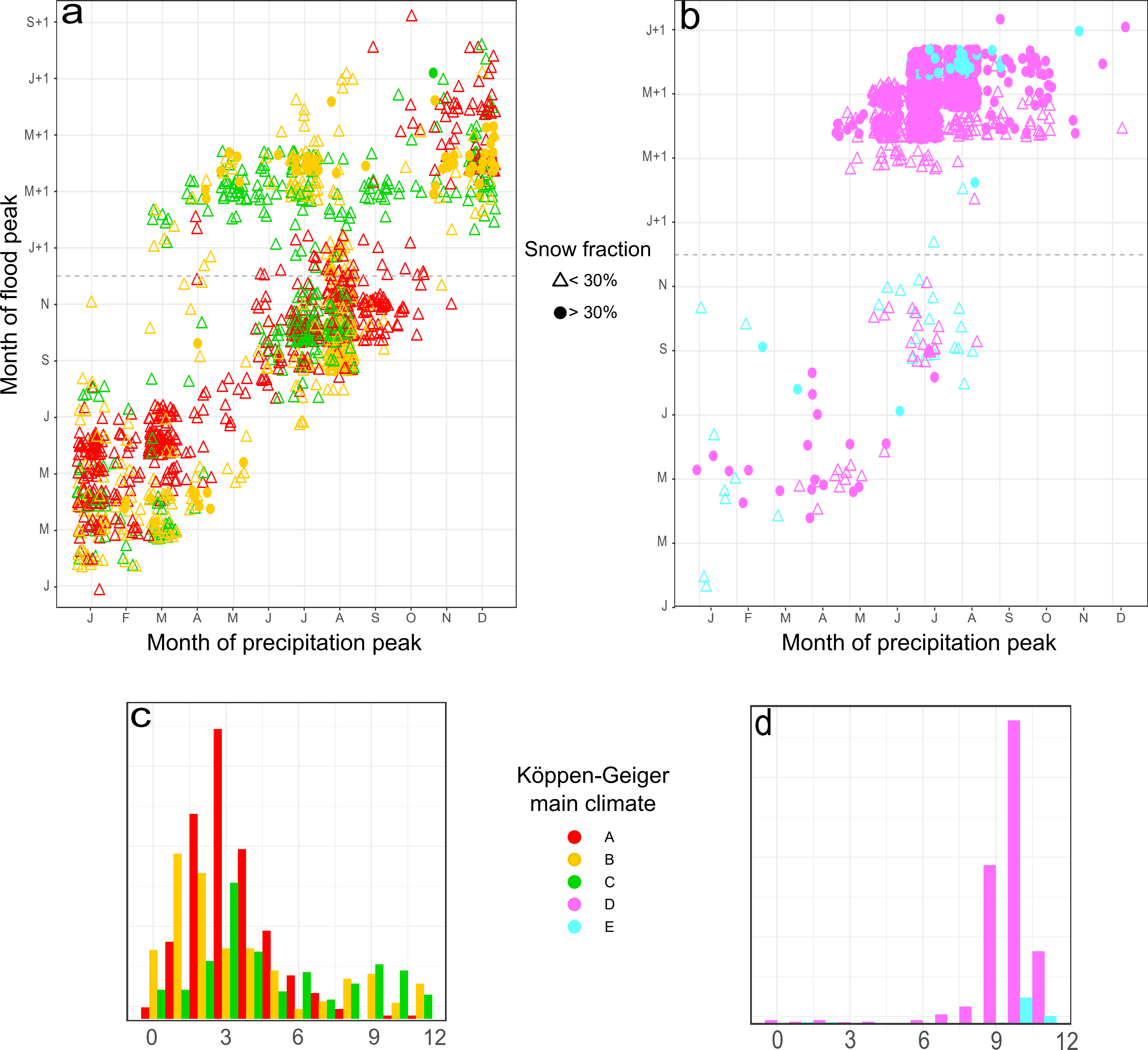
a
b
c
d
Month of flood peak
Month of precipitation peak
S+1
J+1
M+1
M+1
J+1
N
S
J
M
M
J
J F M A M J J A S O N D
Snow fraction
< 30%
> 30%
0 3 6 9 12
Köppen-Geiger main climate
A
B
C
D
E